RESEARCH ACTIVITIES VIII
Laser Research Center for Molecular Science

VIII-A Developments and Researches of New Laser Materials

Although development of lasers is remarkable, there are no lasers which lase in ultraviolet and far infrared regions. However, it is expected that these kinds of lasers break out a great revolution in not only the molecular science but also in the industrial world.

In this project we research characters of new materials for ultraviolet and far infrared lasers, and develop new lasers by using these laser materials.

VIII-A-1 Supercritical-Fluid Cell with Device of Variable Optical Path Length Giving Fringe-Free Terahertz Spectra

SAITOW, Ken-ichi[1]; NISHIKAWA, Keiko[1]; OHTAKE, Hideyuki; SARUKURA, Nobuhiko; MIYAGI, Hiroshi[2]; SHIMOKAWA, Yuji[2]; MATSUO, Hitoshi[3]; TOMINAGA, Keisuke[4]
([1]Chiba Univ.; [2]Gakushuin Univ.; [3]Matsuo Kogyosho, Inc.; [4]Kobe Univ.)

[*Rev. Sci. Instrum.* **71**, 4061 (2000)]

An optical cell suitable for supercritical fluids was constructed for measurements of far infrared absorption spectra with terahertz radiation as a light source. It was designed to withstand temperature up to 400 K and pressure up to 15 MPa. The cell has two characteristic devices; one is diamond windows set in the Brewster angle to the incident far infrared light and the other is a variable optical path length from 30 µm to 20 mm under high pressure conditions. Using the cell, fringe-free spectra of CHF_3 ranging from low-density gaseous states to high-density supercritical ones were measured in a low-energy region of 10–100 cm^{-1}.

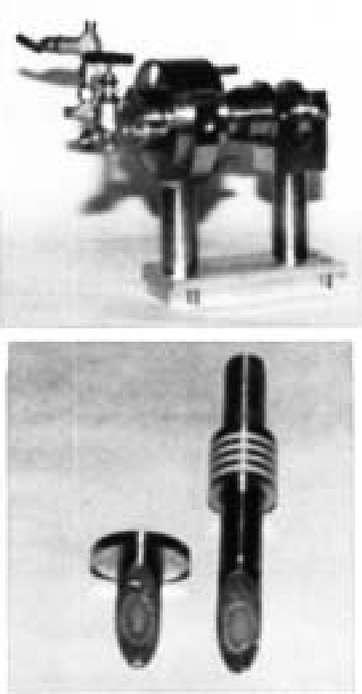

Figure 1. Photographs of an optical cell for far infrared absorption spectra measurements of supercritical fluids. The cell itself is shown in the upper part. The lower part represents flanges with diamond windows set in the Brewster angle, a cylinder, and a V packing.

VIII-A-2 Growth and Characterization of $KMgF_3$ Single Crystals by the Czochralski Technique under CF_4 Atmosphere

SHIMAMURA, Kiyoshi[1]; FUJITA, Tomoyo[1]; SATO, Hiroki[1]; BENSALAH, Amina[1]; SARUKURA, Nobuhiko; FUKUDA, Tsuguo[1]
([1]Tohoku Univ.)

[*Jpn. J. Appl. Phys., Part 1* **39**, 6807 (2000)]

$KMgF_3$ (KMF) single crystals were grown by the Czochralski technique as a new candidate of vacuum-ultra-violet optical materials. The absorption edge of KMF single crystals was 115 nm. The distribution of birefringence in the radial direction was of the order of 10^{-7}. The thermal expansion coefficient of KMF single crystals along the <111> orientation was 1.98×10^{-5} K^{-1}. Together with its excellent mechanical properties, these characteristics show KMF to be superior to the current materials.

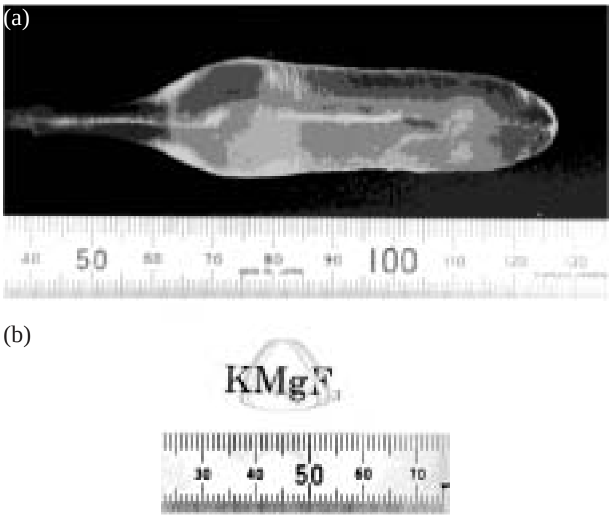

Figure 1. (a) As-grown $KMgF_3$ single crystal of 20 mm diameter pulled along the <111> orientation and (b) $KMgF_3$-wafer cut perpendicular to the growth axis with thickness of 2 mm.

VIII-A-3 Chirped-Pulse Amplification of Ultraviolet Femtosecond Pulses by Use of Ce^{3+}:$LiCaAlF_6$ as a Broadband, Solid-State Gain Medium

LIU, Zhenlin[1]; KOZEKI, Toshimasa; SUZUKI, Yuji; SARUKURA, Nobuhiko; SHIMAMURA, Kiyoshi[2]; FUKUDA, Tsuguo[2]; HIRANO, Masahiro[1]; HOSONO, Hideo[1,3]
([1]ERATO; [2]Tohoku Univ.; [3]Tokyo Inst. Tech.)

[*Opt. Lett.* **26**, 301 (2001)]

Chirped-pulse amplification in the ultraviolet region is demonstrated by use of a broadband Ce^{3+}:$LiCaAlF_6$ laser medium. A modified bow-tie-style four-pass amplifier pumped by 100-mJ, 266-nm pulses from a *Q*-switched Nd:YAG laser has a gain factor of 370 and delivers 6-mJ, 290-nm pulses. After dispersion compensation, the output pulses can be compressed to 115 fs.

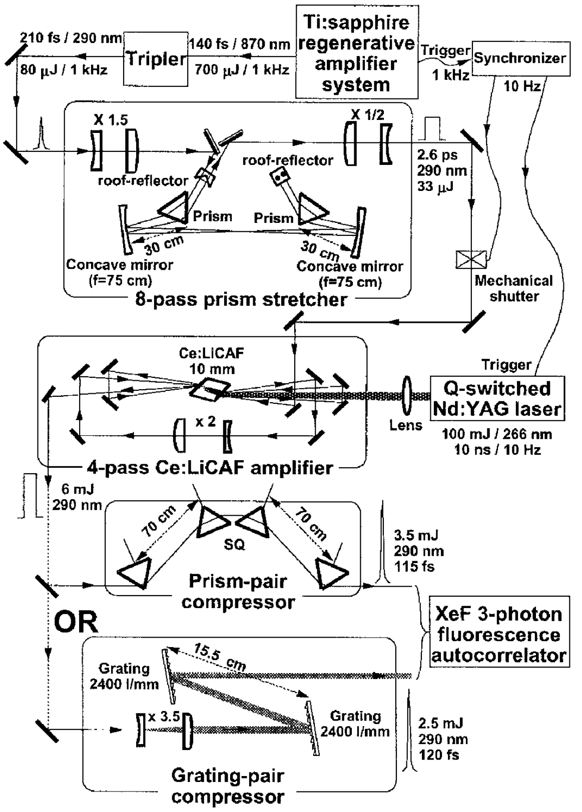

Figure 1. Experimental setup of the Ce:LiCAF CPA laser system. SQ, synthetic quartz.

VIII-A-4 Terahertz Radiation from a Shallow Incidence-Angle InAs Emitter in a Magnetic Field Irradiated with Femtosecond Laser Pulses

ONO, Shingo[1]; TSUKAMOTO, Takeyo[1]; KAWAHATA, Eiji; YANO, Takayuki; OHTAKE, Hideyuki; SARUKURA, Nobuhiko
([1]Sci. Univ. Tokyo)

[*Appl. Opt.* **40**, 1369 (2001)]

The optimized incidence angle and magnetic field direction geometry of an InAs terahertz radiation emitter irradiated with femtosecond laser pulses in a magnetic field is reported. The optimum geometric layout is the magnetic field direction parallel to the semiconductor surface and at an incidence angle that is slightly larger than the Brewster angle. Additionally, we also observed a center frequency shift of terahertz radiation spectrum by changing the incidence angle of the excitation laser.

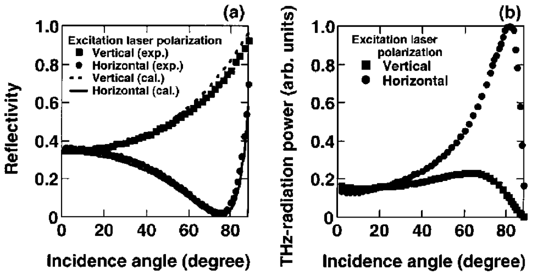

Figure 1. Angular dependence of (a) 800-nm excitation laser reflectivity and (b) THz radiation intensity from InAs. The solid and dotted curves represent the results of our theoretical calculations for $n = 3.729$ and $k = 0.448$.

VIII-A-5 Crystal Growth of Ce-Doped and Undoped $LiCaAlF_6$ by the Czochralski Technique under CF_4 Atmosphere

SHIMAMURA, Kiyoshi[1]; BALDOCHI, Sonia L.[1]; RANIERI, Izilda M.[1]; SATO, Hiroki[1]; FUJITA, Tomoyo[1]; MAZZOCCHI, Vera L.[2]; PARENTE, Carlos B. R.[2]; PAIVA-SANTOS, Carlos O.[3]; SANTILLI, Celso V.[3]; SARUKURA, Nobuhiko; FUKUDA, Tsuguo[1]
([1]Tohoku Univ.; [2]Nucleares-IPEN/CNEN-SP; [3]UNESP)

[*J. Cryst. Growth* **223**, 382 (2001)]

Ce-doped and undoped $LiCaAlF_6$ (LiCAF) single crystals 50 mm in diameter were grown by the Czochralski technique. The formation of inclusions and cracks accompanying the crystal growth was investigated. The dependence of lattice parameters on the temperature was measured for LiCAF and $LiSrAlF_6$ single crystals. Linear thermal expansion coefficients for both these crystals were evaluated. Higher transmission properties for LiCAF single crystals were achieved in the UV and VUV wavelength regions.

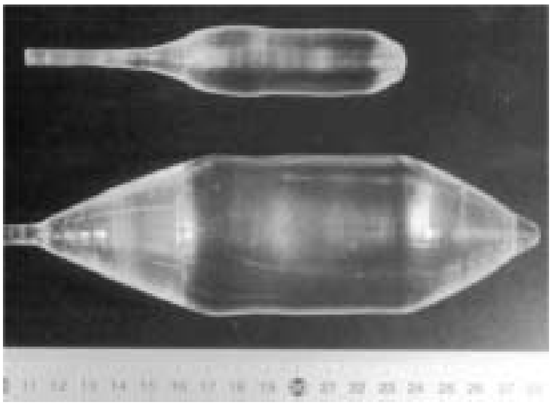

Figure 1. As-grown 2” diameter Ce-doped $LiCaAlF_6$ single crystal.

VIII-A-6 Ultraviolet Femtosecond Pulse Amplification with High Gain Using Solid-State, Broad-Band Gain Medium Ce^{3+}:$LiCaAlF_6$

LIU, Zhenlin[1]; KOZEKI, Toshimasa; SUZUKI, Yuji; SARUKURA, Nobuhiko; SHIMAMURA, Kiyoshi[2]; FUKUDA, Tsuguo[2]; HIRANO, Masahiro[1]; HOSONO, Hideo[1,3]
([1]ERATO; [2]Tohoku Univ.; [3]Tokyo Inst. Tech.)

[*Jpn. J. Appl. Phys., Part 1* **40**, 2308 (2001)]

Femtosecond pulse amplification with high gain in the ultraviolet region has been demonstrated using the solid-state, broad-band crystal Ce^{3+}:$LiCaAlF_6$. With the seed pulses coming from the third harmonic generation of a cw mode-locked Ti:sapphire laser, the confocal, four-pass amplifier pumped by 15-mJ, 266-nm, 10-ns pulses from a Q-switched Nd:YAG laser demonstrates 60-dB gain and delivers 54-µJ, 289-nm, 200-fs, 10-Hz pulses. There is almost no satellite pulse even without any special single-pulse selection.

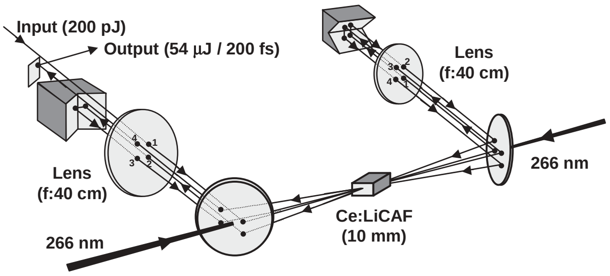

Figure 1. Experimental setup of the confocal, four-pass Ce:LiCAF amplifier. The input is the frequency-tripled output of a cw mode-locked femtosecond Ti:sapphire laser.

VIII-A-7 Terahertz Absorption Spectra of Supercritical CHF_3 to Investigate Local Structure Through Rotational and Hindered Rotational Motions

SAITOW, Ken-ichi[1]; OHTAKE, Hideyuki; SARUKURA, Nobuhiko; NISHIKAWA, Keiko[1]
([1]Chiba Univ.)

[*Chem. Phys. Lett.* **341**, 86 (2001)]

Far infrared absorption spectra of neat supercritical fluoroform (CHF_3) are measured with terahertz (THz) radiation. The spectra covering from 10 to 100 cm^{-1} are obtained at reduced temperature $T/T_c = 1.02$ on densities varied by a factor of 200. As density increases, dominant component of spectra changes from rotational to hindered-rotational motion. However, the change is nonlinear to the density. Such specificity arises from difference between bulk and local densities, and the most enhanced local density is observed near the thermodynamic state of maximum density fluctuation. In the pure fluid system, the relationship between density fluctuation and local density enhancement is experimentally presented.

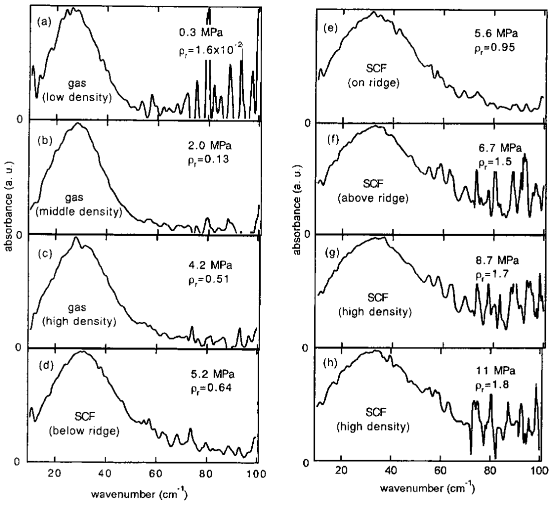

Figure 1. Far infrared absorption spectra of supercritical CHF_3 measured at reduced temperature by $T_r = T/T_c = 1.02$. The (a)–(c) are data below critical pressure (P_c) and (d)–(h) those of above P_c. The (d), (e), and (f) are ones below, on, and above the ridge, respectively. The (g) and (h) are ones at dense supercritical states above the ridge.

VIII-A-8 Observation of New Excitation Channel of Ceriumion through Highly Vacuumultraviolet Transparent LiCAF Host Crystal

KOZEKI, Toshimasa; SUZUKI, Yuji; SAKAI, Masahiro; OHTAKE, Hideyuki; SARUKURA, Nobuhiko; LIU, Zhenlin; SHIMAMURA, Kiyoshi[1]; NAKANO, Kenji; FUKUDA, Tsuguo[1]
([1]Tohoku Univ.)

[*J. Cryst. Growth* **229**, 501 (2001)]

The transmission spectra of $LiCaAlF_6$ (LiCAF) and $LiSrAlF_6$ (LiSAF) are investigated in the ultraviolet (UV) and the vacuum ultraviolet (VUV) region. The transmission edge of LiCAF (112 nm) shows almost the same value as that of LiF. Taking into account difficulties of material processing and polishing due to the cleavage or the hydroscopic nature of LiF, LiCAF is regarded as a more suitable optical material in the UV and the VUV region. Moreover, the new excitation channel around 112 nm is discovered for Ce:LiCAF crystal. This excitation is originated not from absorption of Ceriumions but fromabsorption around the bandgap of the host crystal.

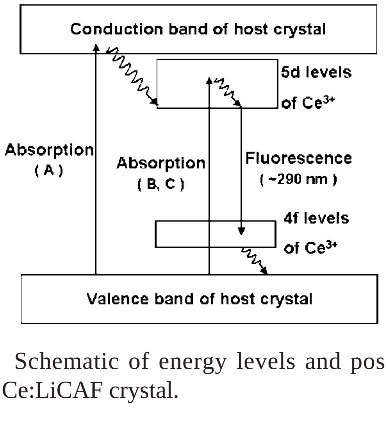

Figure 1. Schematic of energy levels and possible decay channel in Ce:LiCAF crystal.

VIII-A-9 THz-Radiation Emitter and Receiver System Based on a 2 T Permanent Magnet, 1040 nm Compact Fiber Laser and Pyroelectric Thermal Receiver

OHTAKE, Hideyuki; SUZUKI, Yuji; SARUKURA, Nobuhiko; ONO, Shingo[1]; TSUKAMOTO, Takeyo[1]; NAKANISHI, Akio[2]; NISHIZAWA, Seiji[3]; STOCK, Michelle L.[4]; YOSHIDA, Makoto[4]; ENDERT, Heirich[4]
([1]Sci. Univ. Tokyo; [2]Sumitomo Special Metal Co., Ltd.; [3]Shinshu Univ.; [4]Imra America, Inc.)

[*Jpn. J. Appl. Phys.* in press]

Thermal receiver detectable terahertz (THz) radiation is generated from InAs irradiated with a 1040 nm, 80 fs, 180 mW, 48-MHz-repetition-rate mode-locked fiber laser in a 2 T field by a compact permanent magnet. THz radiation is monitored by means of a deuterated triglycine sulfate (DTGS) pyroelectric thermal receiver. DTGS operates at room temperature and does not require time-gating adjustment or cryogen cooling with liquid helium. The THz-radiation emitter system, including the excitation laser head, is almost the same size as a conventional notebook computer.

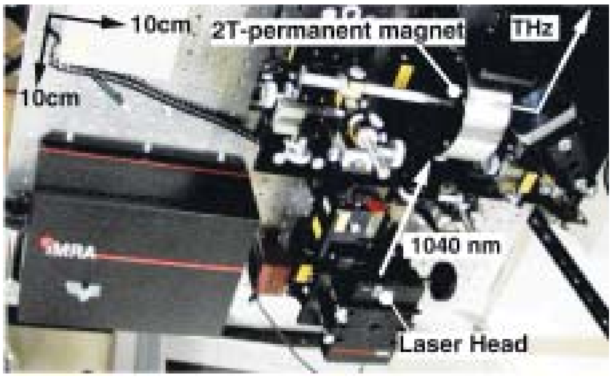

Figure 1. Photograph of THz-radiation emitter system. Laser beam is focused onto the sample with a 2 T permanent magnet.

VIII-A-10 Nanocluster Crystals of Lacunary Polyoxometalates as Structure-Design-Flexible, Inorganic Nonlinear Materials

MURAKAMI, Hidetoshi; KOZEKI, Toshimasa; SUZUKI, Yuji; ONO, Shingo[1]; OHTAKE, Hideyuki; SARUKURA, Nobuhiko; ISHIKAWA, Eri[2]; YAMASE, Toshihiro[2]
([1]Sci. Univ. Tokyo; [2]Tokyo Inst. Tech.)

[*Appl. Phys. Lett.* in press]

Lacunary polyoxometalates, large inorganic, structure-design-flexible, nanocluster crystals are found to have higher optical nonlinearity than KH_2PO_4 (KDP) by the powder second-harmonic-generation (SHG) method. Moreover, the capability of generating ultraviolet radiation down to around 300 nm is found. The basic criteria to design the high nonlinearity are also discovered by the reduction of the molecular symmetry.

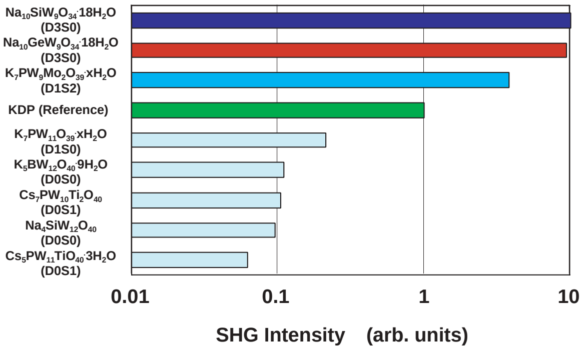

Figure 1. Powder second-harmonic-generation method results using a 1064-nm optical pulse from a Q-switched Nd:YAG laser as the fundamental radiation. Label S denotes the substitution number of metal atom.

VIII-B Development and Research of Advanced Tunable Solid State Lasers

Diode-pumped solid-state lasers can provide excellent spatial mode quality and narrow linewidths. The high spectral power brightness of these lasers has allowed high efficiency frequency extension by nonlinear frequency conversion. Moreover, the availability of new and improved nonlinear optical crystals makes these techniques more practical. Additionally, quasi phase matching (QPM) is a new technique instead of conventional birefringent phase matching for compensating phase velocity dispersion in frequency conversion. These kinds of advanced tunable solid-state light sources, so to speak "Chroma Chip Lasers", will assist the research of molecular science.

In this projects we are developing Chroma Chip Lasers based on diode-pumped-microchip-solid-sate lasers and advanced nonlinear frequency conversion technique.

VIII-B-1 Intra-Cavity Frequency Doubling of a Nd:YAG Laser Passively Q-Switched by Cr^{4+}:YAG Saturable Absorber

PAVEL, Nicolaie; SAIKAWA, Jiro; KURIMURA, Sunao; TAIRA, Takunori

[*Conf. Lasers Electro-Opt.* CTuM27 (2001)]

Frequency doubling of a diode-pumped, passively Q-switched laser could be a convenient method of generating pulsed laser sources in green region. The external-cavity frequency doubling simplifies the cavity design and the green pulses are shorter than that of the Q-switched laser. However, this method is applicable to laser sources that operate with high output powers,$^{1)}$ such that acceptable conversion efficiencies can be realized. On the other hand, intra-cavity frequency doubling made uses of the high peak power that is present inside the cavity, therefore resulting in higher conversion efficiency. A disadvantage of this scheme could be the longer pulses than those produced by a comparable Q-switched laser with no intra-cavity doubling. However, if the accurate pulse width is not critical for application such pulses would reduce the possibility of various types of optical damages. In this work we report a diode-pumped Nd:YAG laser passively Q-switched by a Cr^{4+}:YAG saturable absorber (SA) and intra-cavity frequency doubled by a LBO crystal. The maximum green average power was ~1.0 W, with the laser operating at 3.8 kHz repetition frequency and 87.8-ns pulses duration (263 µJ pulse energy, ~3 kW peak power).

Figure 1 shows a schematic layout of the laser. As pump source we used a 1.55-mm diameter, 0.11 NA fiber-bundled diode (OPC-B030-mmm-FC, OptoPower Co.). We considered a Nd:YAG medium (6-mm diameter, 10-mm length, 1.3-at.%), AR coated at 808 nm on both sides. The plane mirror M1, which was coated for high reflection (HR) at 1.064 mm and high transmission (HT) at 808 nm, was used as the rear mirror of the resonator. The performances of the laser under continuous-wave (CW) operation were first investigated in a plane-plane resonator of 40-mm length. With a flat output mirror of 5% transmission at 1.064 mm we obtained a maximum output power of 8.9 W for an absorbed pump power of 21.0 W, in a laser beam with the M^2 factor of 2.2. The slope efficiency was 48.8%. The performances of the V-type cavity were next determined in CW operation. The plane mirror M^2 was HR coated at 1.064 µm and HT coated at 532 nm. The distances between mirrors M1 and M2, and M2 and M3 were 80 mm and 90 mm, respectively. With a mirror M3 of 50-cm radius and coated as 95% reflectivity at 1.064 µm, a maximum polarized infrared power of 3.8 W for 18.6 W absorbed pump power resulted. The laser beam M^2 factor was 1.14. A 3×3×10 mm^3 LBO crystal was considered for intra-cavity frequency doubling. It was designed for type I second-harmonic generation (critical phase-matching condition), therefore operating at the room temperature. Now M3 was a concave mirror of 50-cm radius and HR coated at both 1.064 mm and 532 nm wavelengths. Thus, 3.2 W green radiation for 18.6 W absorbed pump power in a beam of $M^2 = 1.5$ resulted.

Figure 2 summarize the output properties of the diode-pumped Nd:YAG laser, passively Q-switched by Cr^{4+}:YAG SA and intra-cavity frequency-doubled by LBO. Cr^{4+}:YAG SA crystals with unsaturated transmission T_0 of 90% and 80%, and that were AR coated at 1.064 mm were used. For the SA crystal of 90% initial transmission we obtained an average green power of 1.0 W for the absorbed pump-power of 14.1 W. The laser beam M^2 factor was 1.6. At this pump level the pulse width and the pulse repetition rate were 87.8 ns and 3.8 kHz and the corresponding pulse energy and peak power were 263 µJ and ~3.0 kW. A slightly higher peak power, namely 4.2 kW resulted for the SA of 80% initial transmission: the green average power was ~0.7 W and the pulse width and energy were 50 ns and 209 mJ, respectively. For comparative data on the Cr^{4+}:YAG crystal of 90% initial transmission, the LBO crystal was removed from the resonator and the mirror M3 was replaced by a 90% reflectivity mirror at 1.064 µm. Thus, an infrared maximum average power of 1.1 W resulted at 3.9 kHz and with pulses of 41.5 ns (pulse energy and the peak power were 282 mJ and ~6.8 kW, respectively). As expected, the green pulses were longer than those produced by a comparable Q-switched laser with no intra-cavity doubling. In order to explain the Q-switching results a rate-equation model that accounts for thermally induced effects in Nd:YAG rod, the ratio of the laser-beam area in medium gain to that in SA and its influence on Q-switch performances, and the SA exited state absorption (ESA) contribution was developed. The frequency doubling process was taken into account by introducing a nonlinear loss term in the flux equation rate.$^{2)}$ Following the laser dynamics we have derived analytical expressions that describes the Q-switched pulse energy, peak power, pulse width and repetition rate.3) Using this model a good agreement between the experimental data and theory was obtained for both infrared and second-harmonic regimes.

In summary, we have reported a diode-pumped Nd:YAG laser, passively Q-switched by Cr^{4+}:YAG saturable absorber and intra-cavity frequency-doubled by LBO crystal. The laser produces high beam-quality of 263-µJ energy, 87.8-ns pulses at a pulse repetition rate of 3.8 kHz, for an average power of 1.0 W at 532 nm.

References

1) A. Agnesi, S. Dell'Acqua, E. Piccinini, G. Reali and G. Piccinno, *IEEE J. Quantum Electron.* **34**, 1480 (1998).

2) E.C. Honea, C.A. Ebbers, R. J. Beach, J. A. Speth, J. A. Skidmore, M. A. Emanuel and S.A. Payne, *Opt. Lett.* **23**, 1203 (1998).

3) N. Pavel, J. Saikawa, S. Kurimura, I. Shoji and T. Taira, *Technical Report of Japan Inst. for Electronics, Information and Commun. Engineers (IEICE)* **LQE-65**, 23 (2000).

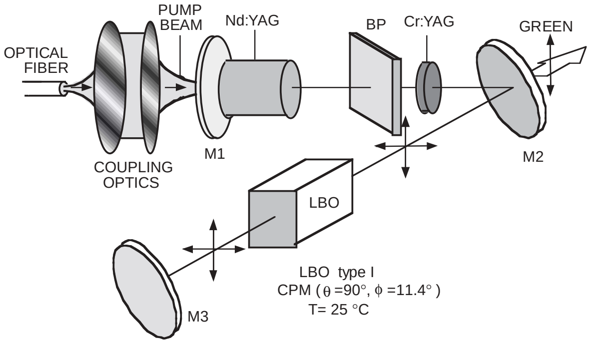

Figure 1. Schematics of the diode end-pumped Nd:YAG laser, passively Q-switched by Cr^{4+}:YAG SA and intra-cavity frequency-doubled by LBO crystal. BP: glass-plate positioned at the Brewster angle.

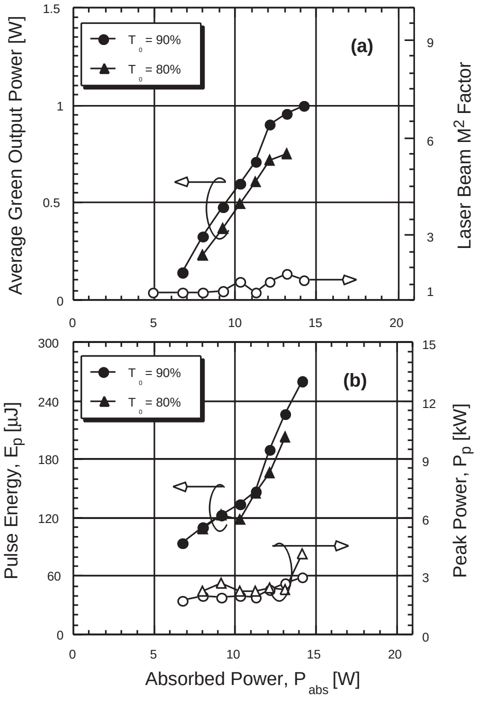

Figure 2. Output properties of diode-pumped Nd:YAG laser, passively Q-switched by Cr^{4+}:YAG and intra-cavity frequency-doubled by LBO. (a) Average power and laser-beam M^2 factor; (b) Pulse energy and pulse peak power.

VIII-B-2 Laser Emission under Resonant Pump in the Emitting Level of Highly Doped Nd Materials

LUPEI, Voicu[1]; TAIRA, Takunori; PAVEL, Nicolaie; SHOJI, Ichiro; IKESUE, Akio[2]
([1]IAP, Romania; [2]JFCC)

[*Conf. Lasers Electro-Opt.* CFD4 (2001)]

Heating effects in the laser active media under pump constitute a major limitation in the construction of highly efficient or high-power solid state lasers. These effects could induce the optical distortion of the resonator or even the physical destruction of the active component. In case of neodymium-doped crystals two major sources exists: the quantum defect between the pump and laser radiation and the non-radiative processes (multiphonon relaxation, down-conversion cross-relaxation on intermediate levels, upconversion from the emitting level $^4F_{3/2}$). While the non-radiative processes constitute a physically inherent loss, the quantum defect can be controlled by the pump and emission wavelengths. In the actual diode pumped Nd laser the pump is accomplished in the $^4F_{5/2}$ level (808.7 nm) and the excitation relaxes by electron-phonon interaction to the components R_1 and R_2 of the emitting level, placed at ~945 and 860 cm^{-1} below the pump level. In absence of laser emission about 39% from the absorbed pump radiation in $^4F_{5/2}$ is transformed into heat in a 1.04 at.% Nd:YAG crystal,1) in accord with a theoretical modeling that accounts for the non-radiative effects on the quantum efficiency.2) In case of an efficient laser emission, when the effect of the non-radiative processes is very small and the heat generation is dominated by the quantum defect the fractional thermal load in this sample is reduced up to about 0.25. However, this figure is much larger than the value of about 0.09 in case of Yb lasers, where the pump is performed in an upper crystal field component of the emitting level.

Pumping in the emitting level or even below it could be a very efficient means for reducing the heating effects in Nd lasers. Thus, in case of Nd:YAG laser, the pump can be performed in the lower component R_1 (11425.5 cm^{-1}) of $^4F_{3/2}$ and the population of the emitting level R_2 (11509 cm^{-1}) can be accomplished by thermal population (at the room temperature about 40% of the population of $^4F_{3/2}$ level is in the R_2 level). The thermallization of the energy levels can be also used for the reduction of the lower quantum defect, between the terminal and the ground level, by pumping in a hot band of the $^4I_{9/2} \rightarrow {}^4F_{3/2}$ absorption. The spectroscopic investigation of various Nd-doped crystals shows that there are many cases when the optical transitions $X_2 \rightarrow R_1$ and $X_3 \rightarrow R_2$ are very close or nearly degenerate, leading to a two- or single-peaked broad feature: at room temperature the population of crystal field components X_2 and X_3 of $^4I_{9/2}$ could be large (in YAG these are 0.246 and 0.178, respectively), leading to a very fairly good absorption of pump. Using these effects (thermal population—assisted pump) is equivalent with a photon cooling. However, since the quantum defect is still positive this is not evidenced as a net cooling of the same sample but only as a reduction of the thermal load. It must be noted that the attempt to observe the laser cooling in Nd:YAG[3)] used the pump with 1.06 micron wavelength in order to excite the tiny fraction of thermal population from the $^4I_{11/2}$ level up to the emitting level $^4F_{3/2}$.

The room temperature absorption spectra of Nd:YAG show these two transitions collected in a two-peaked (885.7 nm and 884.4 nm) broad feature centred around 885 nm. For 1 at.% Nd the absorption coefficient for the two peaks is almost equal, ~1.75 cm^{-1}, *i.e.* much weaker than the 808.7 nm pump transition (~ 9 cm^{-1}). Laser emission has been demonstrated for 1 at.% Nd:YAG crystal[4)] under 885 nm pump. However, the weak absorption of this radiation in the crystal samples precludes the construction of either microchip or high-power lasers.

Recent studies revealed that highly doped Nd:YAG laser components can be fabricated by ceramics technique.[5,6)] The spectroscopic investigation shows that the intensity of the 885 nm band increases linearly with the Nd concentration, the two peaks reaching an absorption coefficient of over 14 cm^{-1} for the 9 at.% sample (Figure 1). At the same time the width of the absorption feature increases by about 25%, from 2.5 nm FWHH to 3.15 nm, by increasing the Nd concentration from 1 to 9 at.%.

In case of Nd:YAG the fractional thermal load is expected to reduce to 0.318 for 1 at.% and to 0.66 for 3.4 at.% Nd under 885 nm pump in absence of laser emission. The most important reduction will be in presence of laser emission, to 0.168 for 1.06 mm emission, *i.e.* a reduction of over 40% from the case with 808 nm pump, and to 0.058 for 940 nm emission, lower than for Yb:YAG laser and with a terminal level (852 cm^{-1}) higher than that of Yb (612 cm^{-1}).

The continuous-wave laser emission in highly doped Nd:YAG ceramics under 885 nm pump was tested with an uncoated active component of 3.4 at.% Nd and 0.87 mm thickness (Figure 2). This was placed in a 25-mm plane-concave resonator with a 50-mm radius output mirror. The 885 nm pump was provided by a Ti:sapphire laser, whose radiation was focussed to a 80 µm diameter in the active medium. For a 95% output mirror reflectivity the laser delivered 42 mW at 1.064 µm for an absorbed pump power of 194 mW; the threshold pump power and the slope efficiency were 87 mW and 37.5%, respectively. With an output mirror reflectivity of 99% the pump threshold dropped to 38 mW but the slope efficiency decreased at 16.7%, while the maximum output power was 27 mW with an optical efficiency of 14%. The improvement of laser performances is under study, by considering coated Nd:YAG ceramic components of optimized size, an improved configuration for the laser resonator as well as an increased pump power.

In conclusion this study shows that the highly doped Nd:YAG ceramics as well as many crystals with high concentrations of Nd ions could be systems of choice for low heat – high power or miniature lasers with hot band (885 nm in case of Nd:YAG) resonant pump.

References

1) T. Y. Fan, *IEEE J. Quantum Electron.* **29**, 1457 (1993).
2) V. Lupei and A. Lupei, *Phys. Rev. B* **61**, 8087 (2000).
3) T. Kushida and J. E. Geusic, *Phys. Rev. Lett.* **21**, 1172, (1968).
4) R. Lavi and S. Jackel, *Appl. Opt.* **39**, 3093 (2000).
5) I. Shoji, S. Kurimura, Y. Sato, T. Taira, A. Ikesue, and K. Yoshida, *Appl. Phys. Lett.* **77**, 939 (2000).
6) J. Lu, M. Prabhu, J. Song, C. Li, J. Xu, K. Ueda, A. A. Kaminskii, H Yagi and T. Yanagitani, *Appl. Phys. B: Lasers Opt.* **71**, 46 (2000).

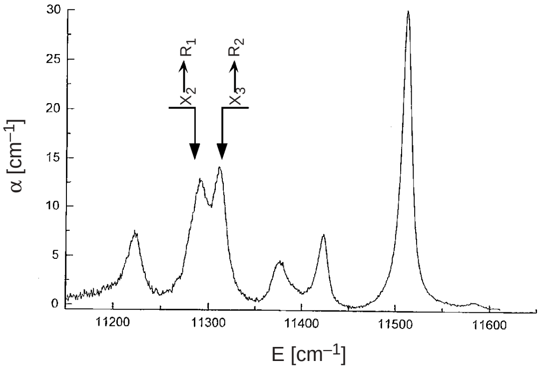

Figure 1. Room temperature $^4I_{9/2} \rightarrow {}^4F_{3/2}$ absorption spectrum of the 9 at.% Nd:YAG ceramics.

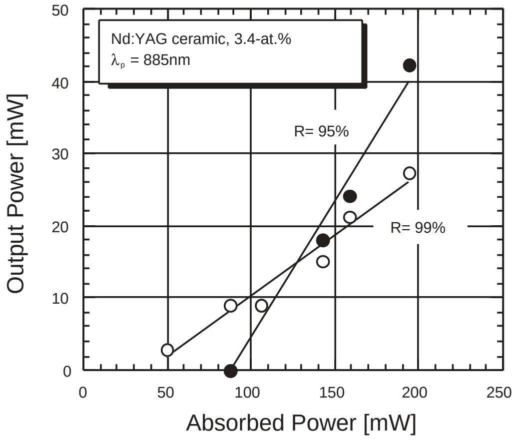

Figure 2. Output to input characteristics for the uncoated 3.4-at.% Nd:YAG ceramic pumped at 885 nm.

VIII-B-3 Thermal Birefringence in Nd:YAG Ceramics

SHOJI, Ichiro; SATO, Yoichi; KURIMURA, Sunao; LUPEI, Voicu; TAIRA, Takunori; IKESUE, Akio[1]; YOSHIDA, Kunio[2]
([1]JFCC; [2]Osaka Inst. Tech.)

[*Conf. Lasers Electro-Opt.* CFD6 (2001)]

Nd:YAG ceramics are promising candidates for high-power and high-efficiency microchip laser materials because highly transparent and highly Nd^{3+}-doped samples are available without degrading thermo-mechanical properties; the thermal conductivity is as high as that of single-crystal YAG even at high Nd^{3+} concentrations. We have succeeded in microchip laser oscillation, in which the output power from a microchip of a 3.4 at. % Nd:YAG ceramic was more than twice as high as that from a same sized microchip of a Nd:YAG single crystal at the same input power. In this work we have investigated thermal birefringence effect in the Nd:YAG ceramics, which should be useful for power scaling.

Thermal birefringence of Nd:YAG ceramics was measured with the pump-probe experiment. A Ti:sapphire laser oscillating at 808 nm was used as the pump beam. The pump beam was focused onto the sample with the radius of 80 µm. On the other hand, linearly polarized He-Ne laser beam was used as the probe beam, and only the depolarized component of the probe beam was detected by use of a polarizer. If the depolarization is defined by the ratio of the depolarized power to the total probe power, dependence of the depolarization on the absorbed pump power for the ceramic and single-crystal samples with various Nd^{3+} concentrations is shown in Figure 1. On the other hand, Figure 2 shows the depolarization as a function of Nd^{3+} concentration at the absorbed pump power of 1000 mW. We found that the depolarization is nearly the same between the ceramic and single-crystal YAG if they have equal Nd^{3+} concentrations. This result indicates that the average of the thermal birefringence induced in the Nd:YAG ceramics is nearly the same with that in the (111)-cut single crystal. Moreover, it was also found that the depolarization became larger in samples with higher Nd^{3+} concentrations even if the same pump power was absorbed. This is mainly attributed to the fact that the fractional thermal loading increases as Nd^{3+} concentration becomes higher. When lasing occurs, on the other hand, thermal birefringence is expected to be greatly reduced because the thermal loading is then independent of Nd^{3+} concentration.

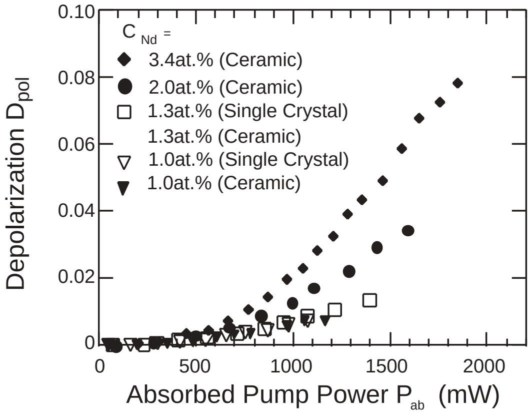

Figure 1. Dependence of the depolarization on the absorbed pump power for the ceramic and single-crystal samples with various Nd^{3+} concentrations.

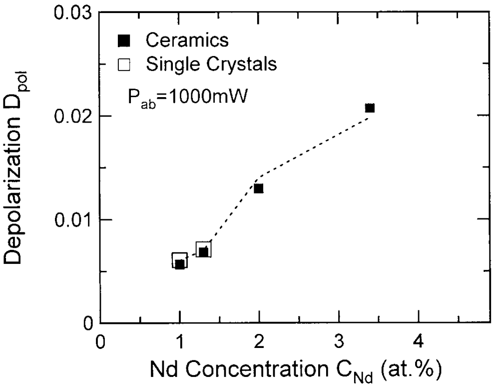

Figure 2. Depolarization as a function of the Nd^{3+} concentration for the ceramic and single-crystal samples at the absorbed pump power of 1000 mW. The dotted curve is the calculated result.

VIII-B-4 In-situ Observation of Fabrication of Nonlinear Optical Wavelength Converter

KURIMURA, Sunao; SHOJI, Ichiro; TAIRA, Takunori; RO, Jung Hoon[1]; CHA, Myoungsi[1]
([1]Pusan Natl. Univ.)

[*Conf. Lasers Electro-Opt.* 3a-Q-22(2001)]

MgO-doped $LiNbO_3$ (MgO:LN) has attracted much attention in quasi-phase-matched (QPM) wavelength conversion due to high resistance to photorefractive damage and low coercive field allowing a large aperture device. Since our first measurement of the coercive field, the crystal has become popular in QPM application and recent works have been verifying high performance of the material. To improve device characteristics, characterization of the domain movement is required for a device with larger aperture. Here we report in-situ monitored poling process and coercive field depending on Mg content in MgO:LN.

The experimental setup for poling is illustrated in Figure 1(a). We used transparent liquid electrode system consisting of transparent plastic blocks and o-rings. Z-cut MgO:LN wafers were sandwiched between two o-rings filled with LiCl electrodes. We observed ferroelectric 180° domains by the electro-optic imaging (EOI) technique under the crossed polarizers. Although EOI technique has a moderate spatial resolution compared with other techniques such as second-harmonic-generation microscope we previously developed, it allows in-situ observation of the poling process with a simple setup. Owing to the small velocity of domain wall in MgO:LN, real-time development was recorded by a commercial video camera. Figure 1(b) shows selected pictures describing the wall movement. Domains with reversed polarization nucleated from the right top corner in the square area directly exposed to the liquid electrode on the +C face. Walls creep very slowly and monitored current has Barkhausen pulses as we reported before. Observed bright spots work as traps of walls, making Barkhausen pulses in current.

We measured coercive fields (Ec) for forward and backward poling in 1mm-thick various crystals with different Mg concentrations of 1–7 mol%. Figure 1(c) presents a significant reduction of coercive field with high doping of Mg. For forward poling, first polarization reversal in fresh wafers, Ec has a minimum value of 4.6 kV/mm at 5 mol%. This corresponds to the lowest defect density at this doping level in the crystal. On the other hand, for backward poling, first polarization reversal after forward poling, Ec decreases monotonically up to 7 mol%. The minimum value we observed here is 2.3 kV/mm at 7 mol%.

In conclusion, we report coercive field dependence on Mg content in LN crystals while observing polarization reversal process simultaneously with poling. Forward coercive field exhibits the minimum value of 4.6 kV/mm at 5 mol% and backward coercive field has the lowest value of 2.3 kV/mm at highest doping level of 7 mol%.

(a)

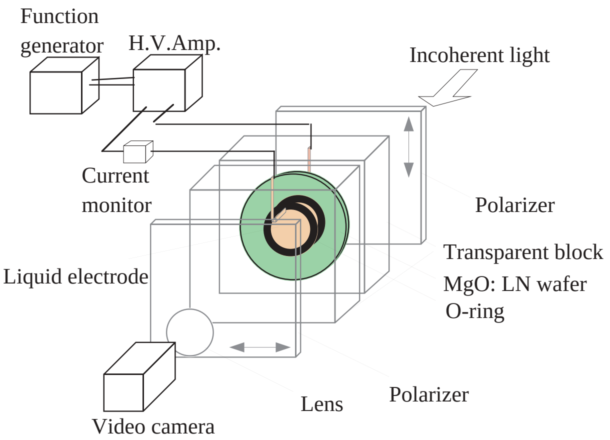

(b)

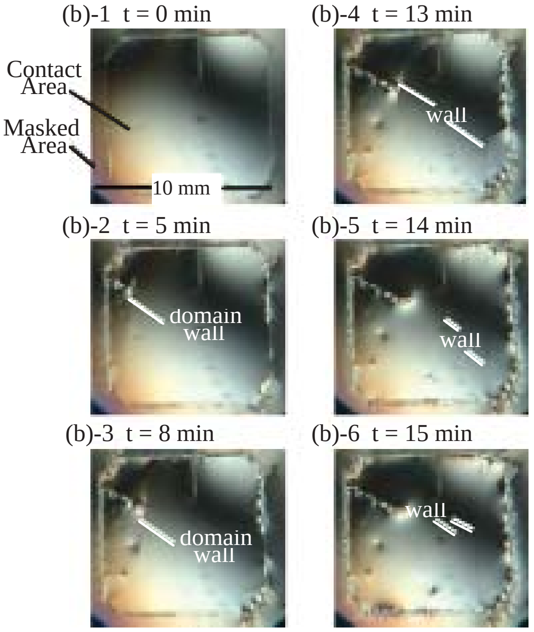

(c)

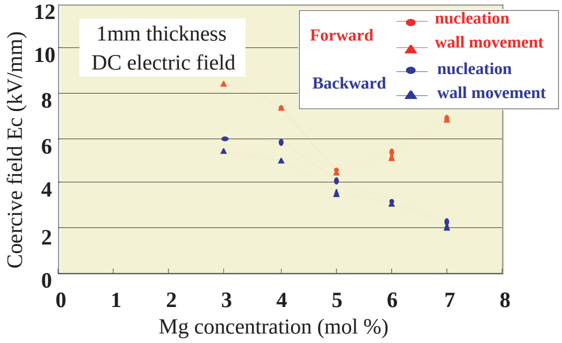

Figure 1. (a) Experimental setup of *in-situ* observation of poling process (b) time development of domains in MgO:LN during electric field poling process (c) coercive field dependence on Mg concentration in MgO:LN.

VIII-B-5 Periodical Twinning in Crystal Quartz for Ultraviolet Nonlinear Optics

KURIMURA, Sunao; FEJER, Martin[1]; SHOJI, Ichiro; TAIRA, Takunori; UESU, Yoshiaki[2]; NAKAJIMA, Hirochika[2]
(*[1]Stanford Univ., USA; [2]Waseda Univ.)*

[*Oyobuturi* **69**, 548 (2000)]

Crystal quartz has low absorption, high chemical stability, and low thermooptic coefficients, attractive for operation in ultraviolet nonlinear optics. Growth techniques are well established because of widespread in surface-acoustic-wave and timing applications, but unfortunately, it doesn't meet the birefringent phase matching condition due to small birefringence, and electric field poling condition due to lack of ferroelectricity. We devised a new poling technique in crystal quartz using mechanical twinning and demonstrated periodical polarity reversal by using thermal stress. Figure 1 shows an observed twin structure with a period of 80 µm, obtained by thermally induced stress between patterned Cr films and a quartz. The Cr patterned substrate was heated to just below Curie temperature in order to attain reasonable film stress and reduce coercive stress. Twins tend to generate from the edge of Cr pattern and the required duty ratio of Cr to the period was more than 0.5. The depth of twins, however, were several microns, indicating not suitable for bulk nonlinear optics. New technique is under development to improve the depth profile of the twins for a practical UV generator.

(a)

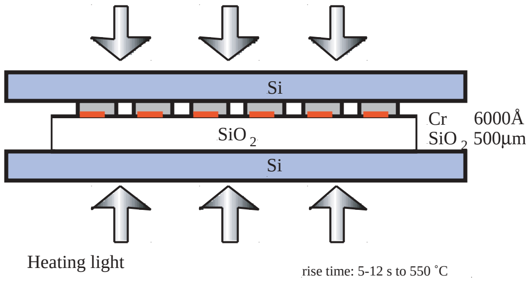

(b)

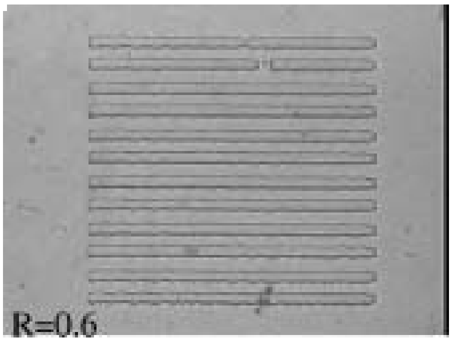

Figure 1. a) patterning method by the thermally induced in-plane stress b) observed periodical twins with a period of 80 µm period. R; duty ratio of the Cr film to the period.

Research Center for Molecular Materials

VIII-C Development of Novel Heterocyclic Compounds and Their Molecular Assemblies for Advanced Materials

Heterocycles containing sulfur and/or nitrogen atoms are useful as components of functional materials since heteroatoms in their rings are helpful to stabilize ions or ion-radical species, and extended π-conjugation decreases Coulombic repulsion. In addition intermolecular interactions caused by heteroatom contacts can be expected to form novel molecular assemblies. In this project new electron acceptors, donors, and donor-acceptor compounds based on heterocycles such as 1,2,5-thiadiazole and 1,3-dithiole were synthesized and their properties including those of the charge-transfer complexes or ion-radical salts were investigated. Unique crystal structures were constructed by using weak intermolecular interactions such as hydrogen bonding or heteroatom contacts. In addition, precisely-defined heterocyclic oligomers containing various types of functional units have been developed, which are a promising building blocks for future molecular nanotechnologies.

VIII-C-1 Linear Hydrogen-Bonded Molecular Tapes in the Co-Crystals of Squaric Acid with 4,4'-Dipyridylacetylene or 1,2-Bis(4-pyridyl)ethylene

ZAMAN, Md. Badruz; TOMURA, Masaaki; YAMASHITA, Yoshiro[1]
([1]IMS and Tokyo Inst. Tech.)

[*Acta Crystallogr., Sect. C: Cryst. Struct. Commun.* **57**, 621 (2001)]

The co-crystals of squaric acid with dipyridyl-type ligands, **1** and **2**, are isomorphous and form in the triclinic crystal system. The co-crystals contain linear and flat hydrogen-bonded molecular tape structures along the [120] direction (Figure 1). The squarate monoanions form a rare ten-membered dimer linked by two intermolecular O–H···O hydrogen bonds [2.511(3) Å for **1** and 2.503(2) Å for **2**]. Each component molecule forms a segregated stack along the c axis. The bond lengths of the squarate monoanion indicate the delocalization of the enolate anion.

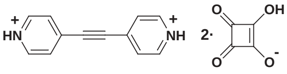

1

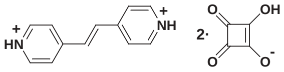

2

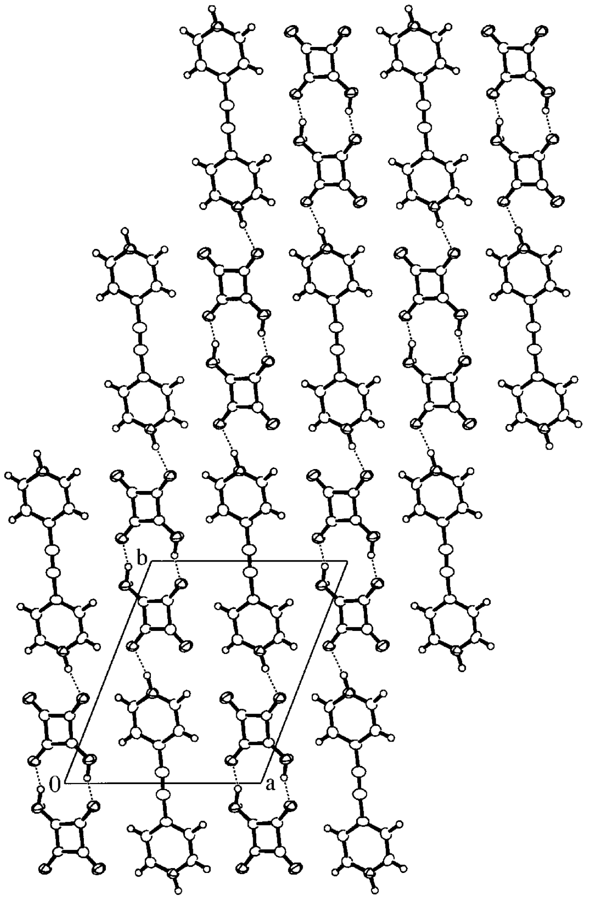

Figure 1. Packing diagram of **1** viewed along the c axis. Dotted lines show the intermolecular hydrogen bonds.

VIII-C-2 One-Dimensional Hydrogen-Bonded Molecular Tapes in 1,4-Bis[(4-pyridinium)ethynyl]-benzene Chloranilate

AKHTARZZAMAN, Md.[1]; TOMURA, Masaaki; YAMASHITA, Yoshiro[2]
([1]GUAS; [2]IMS and Tokyo Inst. Tech.)

[*Acta Crystallogr., Sect. E: Struct. Rep.* **57**, o353 (2001)]

The crystal structure of a 1:1 co-crystal with chloranilic acid and 1,4-bis[(4-pyridyl)ethynyl]benzene contains one-dimensional hydrogen-bonded molecular tapes along the [113] direction, as shown in Figure 1. The molecular tape is nearly flat. The angles between the molecular planes of the chloranilate and the pyridinium ring, and of the pyridinium ring and the benzene ring are 7.3(2)° and 11.8(4)°, respectively. The molecular tapes are connected *via* $R^2_1(5)$ couplings with two intermolecular N–H···O hydrogen bonds [2.609(3) Å and 2.897(4) Å], where both protons of chloranilic acid have transfered to the prydine rings. The overlaps between the chloranilate-pyridinium ring-benzene ring-pyridinium ring-chloranilate are observed in the stacks of the molecular tapes. A short C–Cl··π interaction [Cl···triple bond 3.440(7) Å] exists between the stacks of the molecular tapes. It is 1.7% shorter than the sum of the van der Waals radii of Cl and C*sp*.

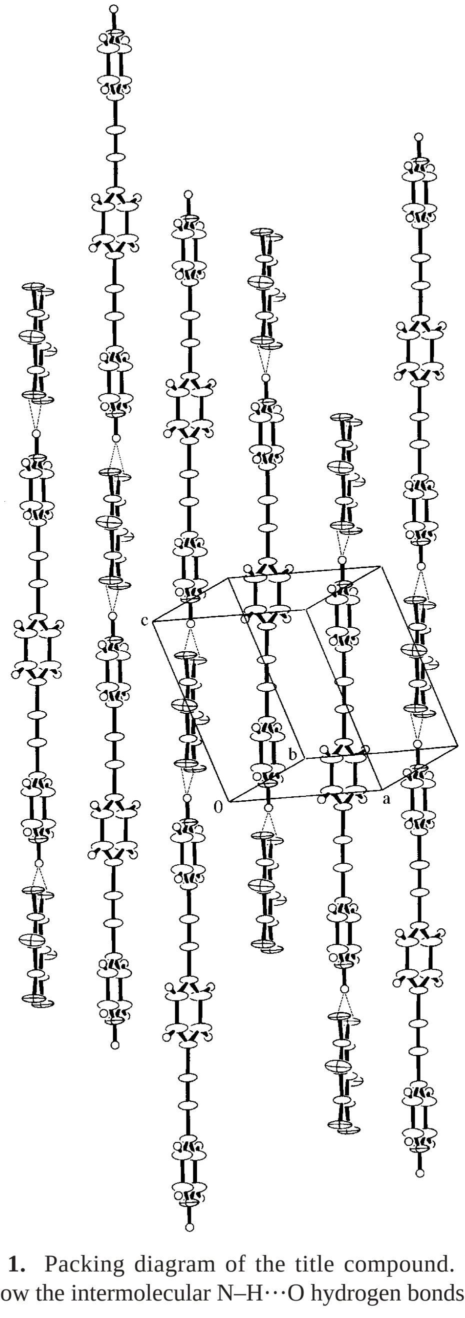

Figure 1. Packing diagram of the title compound. Dotted lines show the intermolecular N–H···O hydrogen bonds.

VIII-C-3 4,7-Bis[(4-pyridyl)ethynyl]-2,1,3-benzothiadiazole and Its Dipyridinium Diperchlorate

AKHTARZZAMAN, Md.[1]**; TOMURA, Masaaki; YAMASHITA, Yoshiro**[2]
([1]GUAS; [2]IMS and Tokyo Inst. Tech.)

[*Acta Crystallogr., Sect. C: Cryst. Struct. Commun.* **57**, 751 (2001)]

A long, rigid and conjugated bridging ligand, 4,7-bis[(4-pyridyl)ethynyl]-2,1,3-benzothiadiazole **1**, and its dipyridinium salt **2** display the bond alternation in the 2,1,3-benzothiadiazole rings, which suggests their quinonoid character. The dipyridinium dication molecules stack along the a axis and form a dimer with short S···N interheteroatom contacts [3.146(4) Å] between the two 1,2,5-thiadiazole rings. The dimer is surrounded by the perchlorate anions with a large number of intermolecular N–H···O and C–H···O hydrogen bonds, as shown in Figure 1.

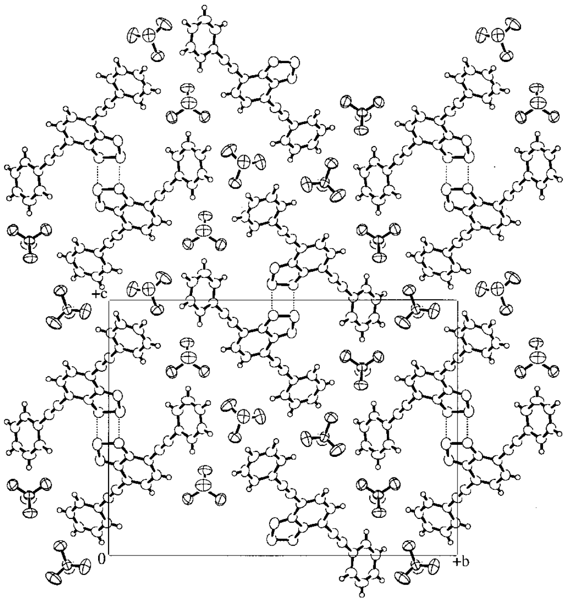

Figure 1. Packing diagram of **2** viewed along the a axis. Dotted lines show the short S···N interheteroatom contacts.

VIII-C-4 One-Dimensional Zigzag Chain Structures with Intermolecular C–H··π and C–H···O Interactions Consisted of Phthalic Acid and Pyridine Derivatives

TOMURA, Masaaki; YAMASHITA, Yoshiro[1]
([1]IMS and Tokyo Inst. Tech.)

[*Chem. Lett.* 532 (2001)]

Crystal structures of co-crystals of phthalic acid with dipyridyl-type ligands, 4,4’-bipyridine or 4,4’-dipyridylacetylene, contain one-dimensional zigzag chain structures connected by intermolecular O–H···N hydrogen bonds. The edge-to-face packing (T-shaped geometry) between phthalic acid and the pyridine rings of the dipyridyl-type ligands is also observed and is stabilized by intermolecular C–H··π and C–H···O interactions. Strong resemblance between the two crystal structures suggests robustness and reproducing ability of the supramolecular synthon formed with phthalic acid and pyridine rings. In this case, a zigzag chain structure seems to be “programmed” to form in a crystal. We have displayed that the supramolecular synthons generated by combination of simple compounds such as phthalic acid and dipyridyl-type ligands can be used in the design of one-dimensional zigzag chain structures and can realize unique preserved crystal structures.

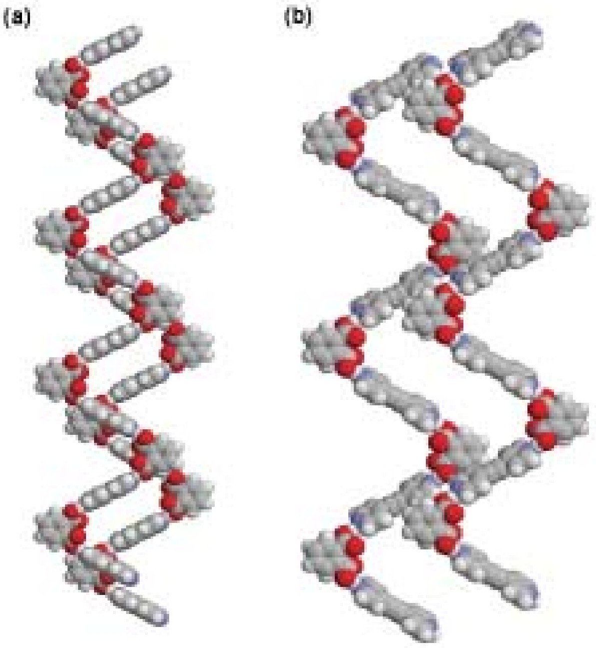

Figure 1. Two one-dimensional zigzag chain structures in the co-crystal of phthalic acid with (a) 4,4’-bipyridine and (b) 4,4’-dipyridylacetylene.

VIII-C-5 Synthesis and Crystal Structures of Decamethylferrocenium Salts of Anilate Anion Derived from Bromanilic Acid, Chloranilic Acid and Cyananilic Acid

ZAMAN, Md. Badruz; TOMURA, Masaaki; YAMASHITA, Yoshiro[1]
([1]IMS and Tokyo Inst. Tech.)

[*Inorg. Chim. Acta* **318**, 127 (2001)]

Four complexes were synthesized using bis(pentamethylcyclopentadienyl)iron Fe(C_5Me_5)$_2$ as an organometallic donor and three anilic acids (2,5-dibromo-3,6-dihydroxy-1,4-benzoquinone; BA, 2,5-dichloro-3,6-dihydroxy-1,4-benzoquinone; CA and 2,5-dicyano-3,6-dihydroxy-1,4-benzoquinone; CNA) as an organic acceptor. The molecular-based structures with different stoichiometric ratios [1:1, 1:1:1(H_2O) and 2:1] of these complexes have been determined by X-ray crystallographic analysis and elemental analysis. These complexes have a one-dimensional alternated stacking arrangement as $D^+A^-D^+A^-$ type. Close contacts between the bromine atoms and oxygen atoms of the BA units are observed in the structure [Fe(C_5Me_5)$_2$](BA) of 1:1 composition. Interestingly, the structures [Fe(C_5Me_5)$_2$](CA)(H_2O) and [Fe(C_5Me_5)$_2$](CNA)(H_2O) of 1:1:1 (H_2O) ratio contain one-dimensional molecular tape structures with the combination of the CA or the CNA units and water molecules *via* O–H···O hydrogen bonds. Different stoichiometric ratios and structures are found from the CNA complexes [Fe(C_5Me_5)$_2$](CNA)(H_2O) and [Fe(C_5Me_5)$_2$]$_2$(CNA).

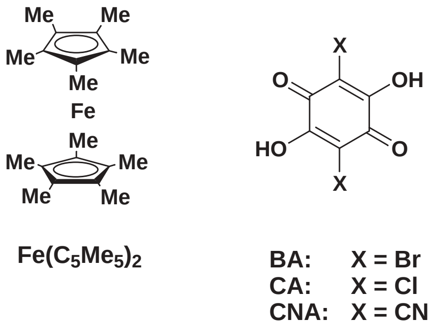

VIII-C-6 Tetrathiafulvalene with a Fused Pyrazine Ring

TOMURA, Masaaki; YAMASHITA, Yoshiro[1]
([1]IMS and Tokyo Inst. Tech.)

[*Acta Crystallogr., Sect. E: Struct. Rep.* **57**, o307 (2001)]

The title compound, 2-(1,3-dithiol-2-ylidene)-2,3-dihydro-1,3-dithia-4,7-diazaindene (pyrazinotetrathiafulvalene) forms a head-to-tail type of π-stacking centrosymmetric dimer with an interplanar distance of 3.59(1) Å. Short S···N interheteroatom contacts [3.10(1) Å] are observed between the two dimers, which form a two-dimensional stacking column along the [101] direction (Figure 1).

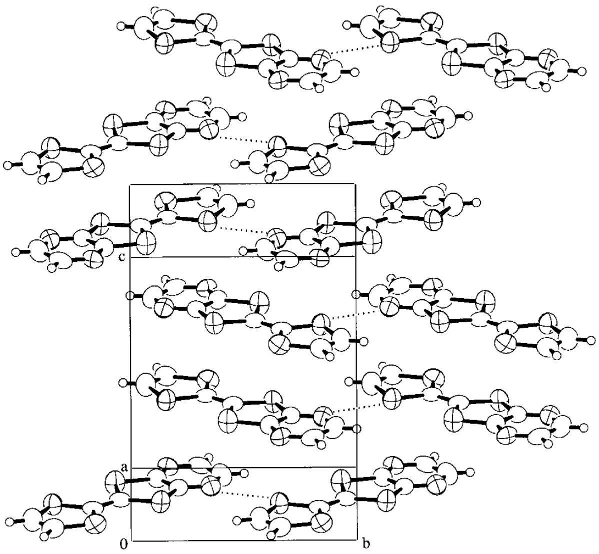

Figure 1. Packing diagram of the title compound. Short S···N interheteroatom contacts are indicated by dotted lines.

VIII-C-7 Hydrogen-Bonded Square Grid-Type Network in the Co-Crystal of Pyrazinotetrathiafulvalene with Chloranilic Acid

TOMURA, Masaaki; YAMASHITA, Yoshiro[1]
([1]IMS and Tokyo Inst. Tech.)

For the development of functional molecular materials, we have designed the hydrogen-bonded square grid-type network using the supramolecular synthon formed with chloranilic acids and heterocyclic compounds with nitrogen. The co-crystal **1** was isolated from an acetone solution of pyrazinotetrathiafulvalene with chloranilic acid. Figure 1 shows the crystal structure of **1**. The square grid-type network with cavities and the segregated unistacks of each molecule are observed. This packing motif is essentially the same as those previously obtained from the co-crystal of chloranilic acid with quinoxaline or phenazine.1) This fact suggests robustness and reproducing ability of the supramolecular synthon formed from chloranilic acid. Moreover, this type of segregated columnar structure is very important for organic conducting materials such as TTF-TCNQ charge transfer complex. The cavities in **1** are occupied by two water molecules. Such guest molecules in the cavities may affect physical properties of organic solids. Crystal data for **1**: $C_{14}H_6Cl_2N_2O_4S_4\cdot(H_2O)_2$, M = 497.35, monoclinic, space group $P2_1/m$, a = 3.867(3), b = 22.419(9), c = 11.675(4) Å, β = 99.27(3)°, V = 999(1) Å^3, Z = 2, T = 296 K, μ(Cu-Kα) = 7.165 mm^{-1}, R_1 = 0.0731 and wR_2 = 0.1841 for 998 data with $I > 2\sigma(I)$.

Reference
1) M. Tomura and Y. Yamashita, *CrystEngComm* 16 (2000).

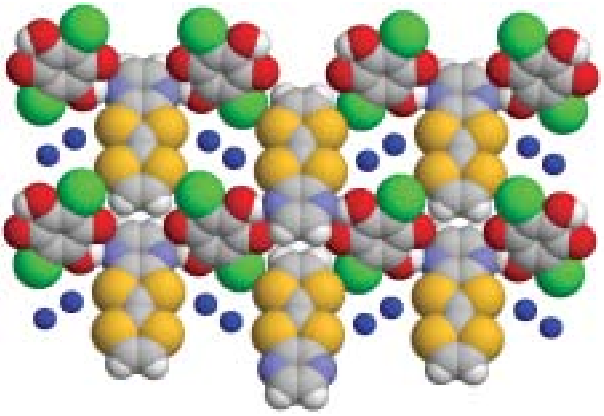

Figure 1. Crystal structure of **1** viewed along the a axis.

VIII-C-8 Hydroxyphenyl Substituted Tetrathiafulvalene Vinylogues Affording Stable Cation Radical Salts with Unusual Crystal Structures

YAMASHITA, Yoshiro[1]**; TOMURA, Masaaki; IMAEDA, Ken-ichi**[2]
([1]IMS and Tokyo Inst. Tech.; [2]IMS and Chubu Univ.)

[*Tetrahedron Lett.* **42**, 4191 (2001)]

TTF vinylogues **1** containing hydroxy phenyl groups were newly prepared. They are stronger electron donors than BEDT-TTF and afforded their cation radical salts as single crystals upon electrochemical oxidation. The X-ray crystallographic analyses of the three cation radical salts **1a**·$Au(CN)_2$·PhCl, **1b**·PF_6, and **1c**·$ReO_4\cdot(H_2O)_8$ have revealed their unusual crystal structures, where p-overlapping and hydrogen bonding play a crucial role in constructing them. The TTF vinylogue skeletons of the salts are planar and the phenyl groups are almost orthogonal to them. The two-dimensional π-overlapping1) of the donor molecules was only found in the structure of **1a**·$Au(CN)_2$·PhCl. The structure of **1c**·$ReO_4\cdot(H_2O)_8$ has a one-dimensional grid-like structure with a void.2) In the structures of the three salts, hydrogen bonding between OH groups and counter anions was observed.

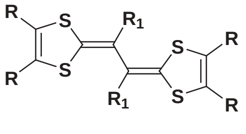

1

a; R, R = $(CH{=}CH)_2$, R_1 = o-OHC_6H_4
b; R, R = $(CH{=}CH)_2$, R_1 = p-OHC_6H_4
c; R, R = SCH_2CH_2S, R_1 = o-OHC_6H_4
d; R, R = SCH_2CH_2S, R_1 = p-OHC_6H_4
e; R, R = SCH_2CH_2S, R_1 = o-$OBzC_6H_4$
f; R, R = SCH_2CH_2S, R_1 = p-$OBzC_6H_4$

References
1) Y. Yamashita, M. Tomura, M. B. Zaman and K. Imaeda, *Chem. Commun.* 1657 (1998).
2) M. Tomura and Y. Yamashita, *CrystEngComm* 14 (2000).

VIII-C-9 A Molecule with a C_1-Homobasketane Framework

TOMURA, Masaaki; YAMASHITA, Yoshiro[1]
([1]IMS and Tokyo Inst. Tech.)

[*Acta Crystallogr., Sect. C: Cryst. Struct. Commun.* **57**, 619 (2001)]

We have carried out the X-ray crystallographic analysis of 6-(1,3-benzodithiol-2-ylidene)-5,7-dimethyl-1,2-diphenylpentacyclo[5.4.0.$0^{2,5}$.$0^{3,11}$.$0^{4,8}$]undecane **1**, which is the C_1-homobasketane derivative with a 1,3-dithiole moiety as the redox part. This is the first example of the crystal structure determination of a molecule with a C_1-homobasketane framework. Compound **1** crystallizes in the triclinic crystal system with one molecule in the asymmetric unit. The molecular structure of **1** is shown in Figure 1. The two cyclobutane rings in the cage are in puckered conformation. Due to the enhanced through-bond interaction of phenyl π systems involving a strained σ bond, the (Ph–)C–C(–Ph) bond length is significantly extended to 1.610(3) Å.

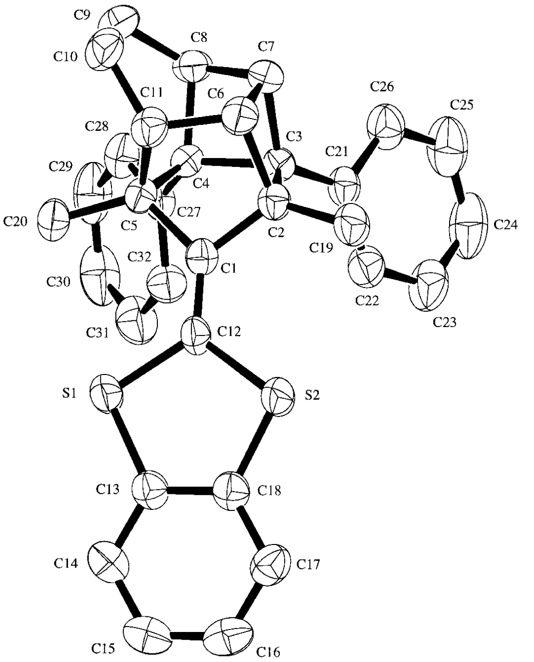

Figure 1. Molecular structure of **1**.

VIII-C-10 Real Space Observation of Individual Conformers of Oligothiophenes on Au(111) Surface

TANAKA, Shoji; YAMASHITA, Yoshiro[1]; YOKOYAMA, Takashi[2]
([1]Tokyo Inst. Tech.; [2]NIMS)

The prototype of a "single molecular device" is now realized for the basic components of digital electronics (rectification, amplification and storage), however, there is still much to be learned about the molecular / supramolecular architecture on solid surface to design practical nanoscopic devices and trier large-scale integration systems. In particular, conformational identification of a π-conjugated molecule has generated a great deal of interest, because the conformational changes in the conjugated skeleton caused by the adsorption on surface will influence appreciably the electronic feature and the self-assembling ability. Here we present a real-space analysis of the molecular conformation and the self-assembling pattern of novel oligothiophenes deposited on the Au(111) surface using UHV low-temperature scanning tunneling microscopy (STM).

The samples are molecular building blocks, **BL-1** and **BL-2**, which have been designed to construct a series of multi-functional molecular wire with insulating mantle as shown in Figure 1. Figure 2a shows the twin-lobe shape of a single **BL-1** molecule, which suggests that this oligomer tends to adsorb with the main-chain parallel to the Au surface. The regular molecular ordering of **BL-1**, however, was not observed as shown in Figure 2b. In the case of the **BL-2**, the STM data shown in Figure 3a reveal that two types of well-ordered domains, *molecular stripes* and *meshes*, evolve on the Au surface. The close-up STM views of these supra-structures as shown Figure 2b-d indicate that the *molecular stripe* and *meshes* consist of *s-trans* and *s-cis* conformer of **BL-2**, respectively. In solution and gas phase, the rapid exchange between the possible conformers of oligomers will occur usually. In molecular crystals, the most stable conformer would be observed predominantly. Our findings demonstrate experimentally that the control of molecular-surface interactions will be one of the key tactics to investigate individual conformers of oligomers and to construct a desired nanostructure based on them.

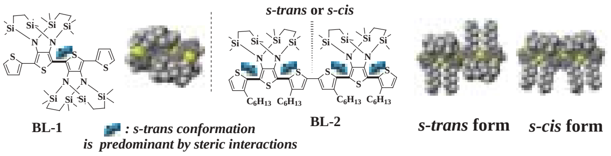

Figure 1. Molecular structure of **BL-1** and **BL-2**.

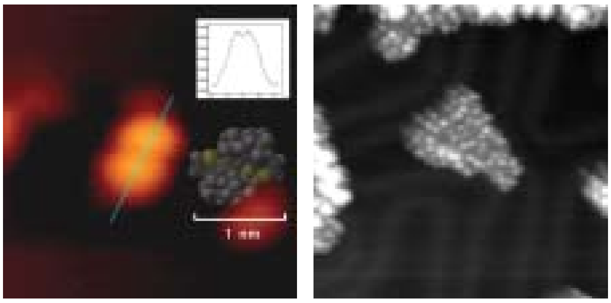

(A) **3.3 nm x 3.3 nm**
(Vs = -2.5 V, It = 5 pA)

(B) **23.5 nm x 23.5 nm**
(Vs = -2.5 V, It = 5 pA)

Figure 2. STM images of **BL-1** on Au(111) surface at 63 K.

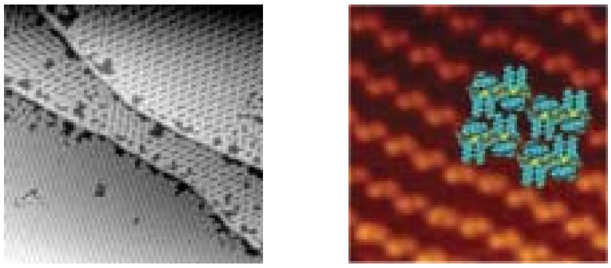

(A) **98 nm x 98 nm**
(Vs = 2 V, It = 5 pA)

(B) **10 nm x 10 nm**
(Vs = -2 V, It = 5 pA)

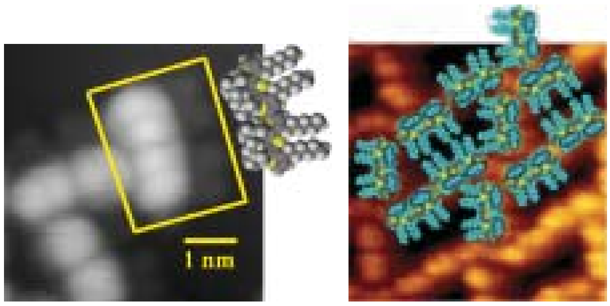

(C) **5nm x5 nm**
(Vs = -2 V, It = 30 pA)

(D) **10 nm x 10 nm**
(Vs = -2 V, It = 5 pA)

Figure 3. STM images of **BL-2** on Au(111) surface at 63 K.

VIII-C-11 Small Bandgap Polymers Involving Tricyclic Nonclassical Thiophene as a Building Block

TACHIBANA, Masamitsu[1]; TANAKA, Shoji; YAMASHITA, Yoshiro[2]; YOSHIZAWA, Kazunari[3]
([1]Kyoto Univ.; [2]Tokyo Inst. Tech.; [3]Kyushu Univ.)

[*J. Phys. Chem. B* submitted]

The band electronic structures of one-dimensional polymers composed of thiophene, pyrrole, and tricyclic nonclassical thiophenes ([1,2,5]thiadiazolo[3,4-*b*]-thieno[3,4-*e*]pyrazine and dithieno[3,4-*b*:3’,4’-*e*]-pyrazine) **1–2** are calculated and analyzed at the extended Hückel level of theory, with the development of highly conducting polymers in mind. The tricyclic nonclassical thiophenes that can impose quinoid-type characters to the resulting polymers are effective building blocks for the preparation of small bandgap polymers. Calculated bandgaps are discussed in view of the frontier crystal orbitals and the bond length alternation of the polymers. The homopolymer of [1,2,5]thiadiazolo[3,4-*b*]thieno[3,4-*e*]pyrazine **1a** that is predicted to have a bandgap of 0.1 eV is a good candidate for an intrinsic conducting polymer without dopants.

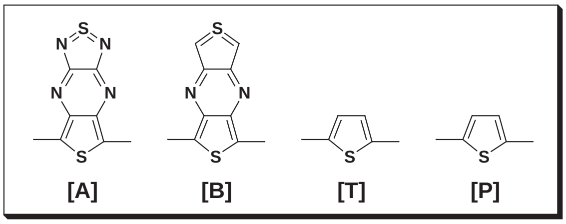

1a: $[A]_n$ 1b: $[AT]_n$ 1c: $[AP]_n$ 1d: $[ATT]_n$ 1e: $[APP]_n$

2a: $[B]_n$ 2b: $[BT]_n$ 2c: $[BP]_n$ 2d: $[BTT]_n$ 2e: $[BPP]_n$

Figure 1. Polymers composed of thiophene, pyrrole, and tricyclic nonclassical thiophenes.

VIII-C-12 Prospects of Single Molecule Devices for Future High Performance Infromation Technologies

WADA, Yasuo[1]; TSUKADA, Masaru[2]; FUJIHIRA, Masamichi[3]; MATSUSIGE, Kazumi[4]; OGAWA, Takuji[5]; HAGA, Masa-aki[6]; TANAKA, Shoji
([1]Hitachi Ltd., Adv. Res. Lab.; [2]Univ. Tokyo; [3]Tokyo Inst. Tech.; [4]Kyoto Univ.; [5]Ehime Univ.; [6]Chuo. Univ.)

[*Jpn. J. Appl. Phys.* **39**, 3835 (2000)]

Current information technologies use semiconductor devices and magnetic/optical discs, however, it is foreseen that they will all face fundamental limitations within a decade. This paper reviews the prospects and problems of single molecule devices, including switching devices, wires, nanotubes, optical devices, storage devices and sensing devices for future information technologies and other advanced applications in the next paradigm. The operation principles of these devices are based on the phenomena occurring within a single molecule, such as single electron transfer, direct electron-hole recombination, magnetic/charge storage and regand-receptor reaction. Four possible milestones for realizing the Peta (10^{15})-floating operations per second (P-FLOPS) personal molecular supercomputer are described, and the necessary technologies are listed. These include, (1) two terminal conductance measurement on single molecule, (2) demonstration of two terminal molecular device characteristics, (3) verification of three terminal molecular device characteristics and (4) integration of the functions of “molecular super chip.” Thus, 1000 times higher performance information technologies would be realized with molecular devices.

VIII-D Designing Artificial Photosynthesis at Molecular Dimensions

Photosynthesis is one of the finest piece of molecular machinery that Nature has ever created. Its ultrafast electron transfer and following well-organized sequence of chemical transformation have been, and will continue to be, challenging goals for molecular scientists. We are trying to mimic the function of photosynthesis by assembling molecular units that perform individual physical/chemical action. The molecular units include porphyrins, redox active organic molecules, and transition metal complexes. Our ultimate goal is to design artificial molecular systems that effect multiple chemical reactions triggered by light on the basis of molecular rationale.

Last year we focused our attention on combining “redox pool” with photoinduced electron transfer.

VIII-D-1 Synthesis and Photochemical Reactions of Multistep Redox Polymer Containing Porphyrin and Metalocenes

HINO, Takami[1]; ITO, Hajime; NAGATA, Toshi
([1]Kyoto Univ.)

Photoinduced electron transfers involving porphyrins are widely studied, but utilizing the high-energy radical ion pairs for driving chemical reactions remains to be a great challenge. One of the missing features in artificial photosynthetic models based on organic molecules is the function of redox pool—that receives the oxidizing and/or reducing equivalents from the photogenerated ion pairs and retains them sufficiently long until the substrates for chemical reactions are ready. This feature is essential for photosynthetic processes to be successful, because the photogenerated high-energy states are otherwise too short-lived to cooperate with (comparatively slow) chemical reactions. In biological systems various electron-carrying substances (proteins like soluble cytochromes, or cofactors like quinones) play the role, whereas in many artificial systems solid particles with electronic band structure (metal or semiconductor nanoparticles) do that. It should be an important research topic to develop redox pools with organic and organometallic substances and utilize in molecule-based artificial photosynthetic systems.

With this goal in mind, we prepared polysiloxanes containing ferrocene and porphyrin moieties (Figure 1). The ferrocenes are present in 20-fold excess of porphyrins, so that they can serve as ‘electron pool’ that retains photogenerated holes on porphyrin moieties.

The desired polymer **1** was prepared by hydrosilylation of a mixture of vinylferrocene and (4-pentenyloxy)phenyl substituted porphyrin with poly(methylhydro)siloxane catalyzed by hexachloroplatinic acid (Figure 2). Purification by reprecipitation from tetrahydrofuran/methanol followed by gel permuation chromatography yielded the product with reasonably narrow size distribution (M_w/M_n = 1.4). The cyclic voltammogram of **1** is shown in Figure 3; a large peak of ferrocenes and two small peaks of porphyrins are observed as expected.

The photoreaction of **1** with quinones were examined. We previously reported the reductive silylation of quinones photocatalyzed by porphyrins (H. Ito, T. Hino, T. Nagata, submitted; see also Annual Review 2000). As the photoreduced product of quinones are trapped by silylating reagents, this reaction can be used to continuously pick up electrons from donor molecules. Indeed, irradiation with visible light of a mixture of the polymer **1**, 2,3,5,6-tetramethyl-1,4-benzoquinone, Me_3SiCl and pyridine in tetrahydrofuran/N,N-dimethylformamide gave the oxidized form of **1** (*i.e.* the ferrocene moieties were converted to ferrocenium) together with the reduced product, 2,3,5,6-tetramethyl-1,4-bis(trimethylsiloxy)benzene (Figure 4). The full identification, as well as the follow-up chemistry (*i.e.* reducing back to the original form) of the oxidized form of **1** is currently under way.

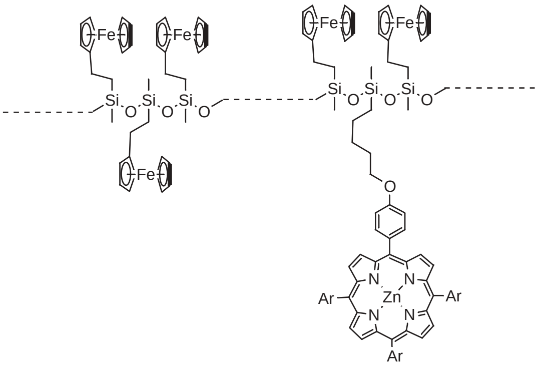

Figure 1. A redox polymer with a photoactive moiety.

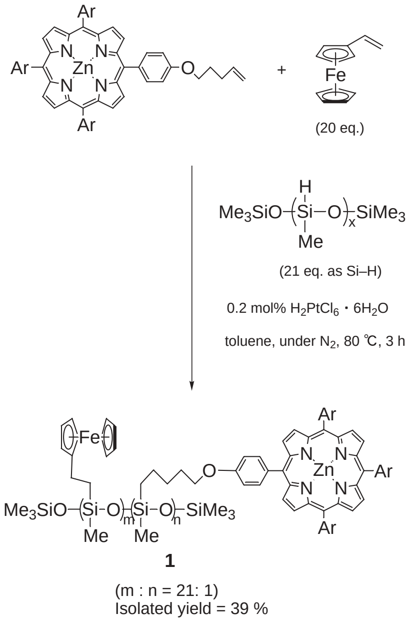

Figure 2. The synthesis of polymer **1**.

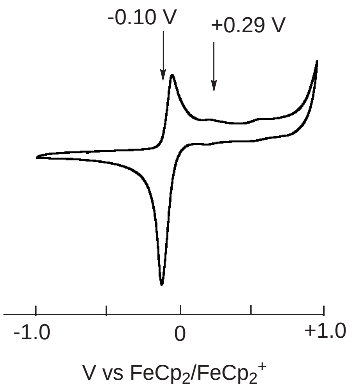

Figure 3. The cyclic voltammogram of polymer **1**. Conditions: CH_2Cl_2 with 0.1 M Bu_4NClO_4, Pt working electrode.

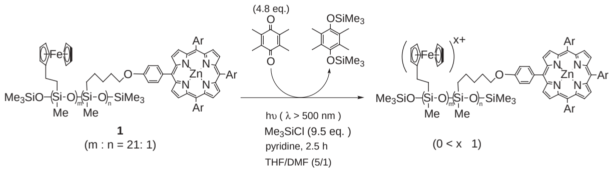

Figure 4. The photoreaction of polymer **1** with quinone and Me_3SiCl.

VIII-E Development of New Metal Complexes as Redox Catalysts

Redox catalysis is an important field of chemistry which translates a flow of electron into chemical transformation. It is also one of the requisites for artificial photosynthesis. This project of ours aims at developing new metal complexes that perform redox catalysis at low overpotential. Last year we focused our attention to developing terdentate ligands with strong donor character. 2,2’:6’,2”-Terpyridine has been the ligand of choice in this field, but our study has now revealed that 2,2’:6’,2”-terpyridine-1,1”-dioxide is also a good candidate for developing new catalysts.

VIII-E-1 Synthesis of Terpyridine-based Binary Ligands and Their Metal Complexes

ITO, Kaname; NAGATA, Toshi; TANAKA, Koji

[*Inorg. Chem.* in press]

In recent years, metal complexes of 2,2’:6’,2”-terpyridine (terpy) and their derivatives are gaining considerable attention as electrochemical catalysts. Derivatives of terpyridine are particularly suitable for electrocatalytic applications because they are chemically robust and form stable complexes with a wide variety of transition metals. On the other hand, the syntheses of terpyridine derivatives are often so troublesome that it is difficult to tune the electrochemical behavior of the metal complexes.

The *N*-oxides of pyridines are promising ligands that are easily derived from pyridine compounds by one-step peracid oxidation. Metal complexes of pyridine *N*-oxide and 2,2’-bipyridine 1,1”-dioxide are numerous, whereas the *N*-oxides of terpyridine have been much less studied. Only a few reports were published on the metal complexes of 2,2’:6’,2”-terpyridine 1,1’,1”-trioxide (terpyO_3).

We prepared a series of first-row transition metal complexes of 2,2’:6’,2”-terpyridine 1,1”-dioxide (terpyO_2) are reported. Four new bis complexes [M(terpyO_2)]X_2 (M = Mn(II), Fe(II), Co(II) and Ni(II); X = ClO_4^- and BF_4^-) and one mono complex [Cu(terpyO_2)(H_2O)]$(ClO_4)_2$ were isolated and characterized, and electrochemical properties were examined. The crystal structure of the Fe(II) complex [Fe(terpyO_2)$_2$]$(ClO_4)_2$ is shown in Figure 1. The ligands have non-planar conformations with an approximate C_2 symmetry, which makes the overall symmetry of the complex cation approximately D_2. The Ni(II) complex [Ni(terpyO_2)$_2$]$(ClO_4)_2$ was isostructural with the Fe(II) complex. The X-ray structure of the Cu(II) complex was also examined (Figure 2), and it was revealed that the Cu(II) ion was square-planar with the terdentate terpyO_2 ligand whose conformation was similar as in the Fe(II) and Ni(II) complexes.

The cyclic voltammograms of the four bis complexes revealed that the M(III)/M(II) redox potentials of the Mn(II), Fe(II) and Ni(II) complexes showed negative shifts (–0.77 to –0.24 V) compared to the terpyridine complexes, whereas the potential of the Co(II) complex showed a slightly positive shift (+0.03 V). The Fe(II) complex is particularly interesting, because the low $E_{1/2}$ value and the ease of ligand exchange (revealed by ESI-MS) make the complex promising for application as a redox catalyst. Also worth noting is the Mn(II) complex, for which another reversible wave corresponding to the Mn(IV)/Mn(III) couple was observed. The electrocatalytic properties of the terpyO_2 complexes is now being investigated.

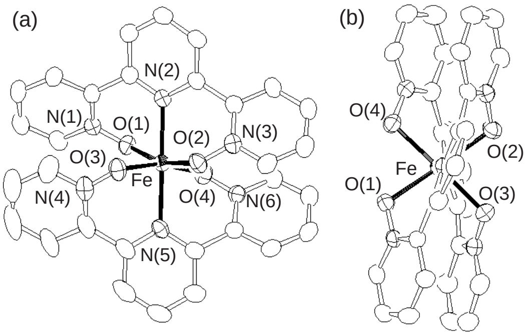

Figure 1. ORTEP view (50% probability ellipsoids) of the complex cation $[Fe(terpyO_2)_2]^{2+}$.

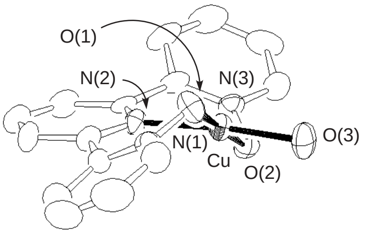

Figure 2. ORTEP view (50% probability ellipsoids) of the complex cation $[Cu(terpyO_2)(H_2O)]^{2+}$.

VIII-F Development of Organic n-Type Semiconductors for Molecular Thin-Film Devices

Organic light-emitting diodes (OLEDs) and field-effect transistors (FETs) based on π-conjugated oligomers have been extensively studied as molecular thin-film devices. Organic n-type semiconductors with low electron-injection barriers and high electron mobilities are required for highly efficient OLEDs and n-type FETs. Radical anions of an n-type semiconductor have to be generated easily at the interface with a metal electrode (electron injection), and electrons must move fast in the layer (electron mobility). Compared with organic p-type semiconductors, organic n-type semiconductors for practical use are few and rather difficult to develop. Recently, we found that perfluorinated oligomers are efficient electron-transport materials for OLEDs.

VIII-F-1 Tetradecafluorosexithiophene: The First Perfluorinated Oligothiophene

SAKAMOTO, Youichi; KOMATSU, Shingo; SUZUKI, Toshiyasu

[*J. Am. Chem. Soc.* **123**, 4643 (2001)]

Perfluoro-a-sexithiophene (**PF-6T**) was synthesized by the fluorination of thienyllithiums with *N*-fluoro-*N*-(phenylsulfonyl)benzenesulfonamide and the Stille and Ullmann couplings. **PF-6T** is an orange crystalline solid and slightly soluble in $CHCl_3$ and aromatic solvents such as toluene. Its structure was determined by EI-MS, elemental analysis, and X-ray crystallography. **PF-6T** exhibits bluish-green photoluminescence in solution and an orange emission in the solid state. A sharp melting endotherm was observed at 286 °C by DSC. The differential pulse voltammogram (DPV) in 1,2-dichlorobenzene showed that the redox potentials of **PF-6T** shifted positively relative to α-sexithiophene (**6T**). Single crystals of **PF-6T** were successfully grown by slow sublimation at 270 °C under a flow of 1 atm of argon. The structure of **PF-6T** is *all-trans* and planar as observed for **6T**. **PF-6T** adopts a π-stack structure with face-to-face molecules. This is quite different from the herringbone structure of **6T**, in which π-π interactions between neighboring molecules are minimized to reduce the repulsion between π-orbitals. High electron mobility is expected along the π-π stacking direction. Fabrication of n-type FETs with this new material is currently underway.

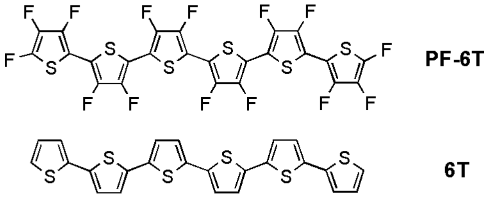

Figure 1. Perfluoro-α-sexithiophene and α-sexithiophene.

VIII-F-2 Highly Efficient Phosphorescence from Organic Light-Emitting Devices with an Exciton-Block Layer

IKAI, Masamichi[1]; TOKITO, Shizuo[1]; SAKAMOTO, Youichi; SUZUKI, Toshiyasu; TAGA, Yasunori[1]
([1]Toyota Central R&D Labs.)

[*Appl. Phys. Lett.* **79**, 156 (2001)]

One of the keys to highly efficient phosphorescent emission in organic light-emitting devices is to confine triplet excitons generated within the emitting layer. We employ “starburst” perfluorinated phenylenes ($C_{60}F_{42}$) as a both hole- and exciton-block layer, and a hole-transport material 4,4’,4”-tri(*N*-carbazolyl) triphenylamine as a host for the phosphorescent dopant dye in the emitting layer. A maximum external quantum efficiency reaches to 19.2%, and keeps over 15% even at high current densities of 10–20 mA/cm^2, providing several times the brightness of fluorescent tubes for lighting. The onset voltage of the electroluminescence is as low as 2.4 V and the peak power efficiency is 70–72 lm/W, promising for low-power display devices.

VIII-G The Effects of the 2D Spin-Echo NMR Experiment on a Solid-State Homonuclear Spin-1/2 Pair

The 2D spin-echo NMR experiment can reintroduce the influence of homonuclear dipolar interactions average out by magic-angle sample spinning (MAS).

VIII-G-1 Novel Structure Discovered on Two-Dimensional Spin-Echo NMR Spectra for a Homonuclear Spin-1/2 Pair in Rotating Solids

KUWAHARA, Daisuke; NAKAI, Toshihito[1]; ASHIDA, Jun[2]; MIYAJIMA, Seiichi
([1]Tokyo Univ. Agric. Tech.; [2]Kyoto Univ.)

Two-dimensional (2D) spin-echo NMR experiments have been carried out on polycrystalline [2,3-$^{13}C_2$]-*L*-alanine under magic-angle sample spinning (MAS) conditions, so that two unusual resonance lines emerged along the F_1 axis. Theoretically it was found that the line positions were determined by the sample spinning frequency and the isotropic chemical-shift difference (*Chem. Phys. Lett.* **305**, 35 (1999)). Stimulated by the result, we carried out the 2D NMR experiment using a sufficiently small t_1 increment in order to enlarge the spectral width of the F_1 domain. As a result, we found many more resonance lines on a spectrum sliced along the F_1 axis. The line distribution had a very unique and interesting structure. To elucidate the line positions theoretically, the signal for the 2D spin-echo experiment performed with any t_1 increment was calculated analytically for a homonuclear two-spin-1/2 system undergoing MAS. We showed that virtually six resonance lines (exactly twelve resonance lines) occurred on a spectrum sliced along the F_1 axis. In addition, it was demonstrated that the intensities of some resonance lines were largely dependent on the dipolar interaction. The 2D spin-echo experiment for a solid-state homonuclear two-spin system was found to have the capability of extracting information concerning the dipolar tensor under MAS conditions.

VIII-H Rotational Echo Double Resonance (REDOR) Experiments with Overtone Adiabatic Inversion Pulses

The effect of overtone adiabatic inversion pulse on solid-state ^{14}N spins was investigated.

VIII-H-1 The Observation of REDOR Phenomenon for Solid-State ^{13}C-^{14}N spin Systems with the Help of Overtone Adiabatic Inversion Pulses

KUWAHARA, Daisuke

We applied overtone adiabatic inversion pulses to ^{13}C-^{14}N spin systems in powdered *L*-alanine undergoing MAS in order to observe REDOR phenomenon. The damping of ^{13}C resonance line intensities was compared with that corresponding to the REDOR experiments with normal RF pulses having a constant frequency. We tried to establish the theoretical treatment for the REDOR experiments with adiabatic inversion pulses.

Equipment Development Center

VIII-I Development of "IMS Machines"

The technical staff of the Equipment Development Center is partly engaged in planning, researching, designing and constructing "IMS machines." This machine, crowned with the acronym of the Institute for Molecular Science, is a high-tech experimental instrument, with emphasis on new technical idea and co-operative work with members inside and outside the Institute including those in industries. We collect suggestions of new instruments once every year from all of the members of IMS.

In this fiscal year, 2000, two project themes (1 thorough 2) were adopted as IMS machines. IMS machine projects 3 (IMS machine 1999) was completed, and project 4, 5 (IMS machine 1999) are under way.

1. **A Novel Method for Intensefying Oriented Molecular Beam: Electrostatic Honeycomb Filed**
   (proposed by SHIMIZU Yuichiro, CHE Dock-Chill, HASHINOKUCHI Mitihiro, SUZUI Mitsukazu, WATANABE Michio and KASAI Toshio)
2. **The Development of a Photoion and Photoelectron CMOS Imaging Detector with High Repetition Rates**
   (proposed by GEJO Tastuo and YOSHIDA Hisashi)
3. **Vacuum-Chamber-Based High Voltage Application Apparatus to Fabricate Wide-Range Nonlinear Optical Wavelength Converters**
   (proposed by KURIMURA Sunao, TAIRA Takunori, KOBAYASHI Kazuhiro and SUZUI Mitukazu)
4. **Sorption-Pump-Type Large-Scale Dilution Refrigerator**
   (proposed by SHIBAYAMA Hideo and KONDOH Takuhiko)
5. **High-Speed Array Detector**
   (proposed by Kazuo WATANABE and Hisashi YOSHIDA)

VIII-I-1 A Novel Method for Intensefying Oriented Molecular Beam: Electrostatic Honeycomb Field

SHIMIZU, Yuichiro; CHE, Dock-Chil; HASHINOKUCHI, Mitihiro[1]; SUZUI, Mistukazu; WATANABE, Michio; KASAI, Toshio[1]
([1]IMS and Osaka Univ.)

By using electrostatic hexapole field, "steric effect" in chemical reactions has been extensively studied.[1] This method enables us to control reactant molecular orientation prior to collision. Intensity of oriented molecular beam, however, inevitably becomes weaker than its un-oriented molecular beam by more than one order of magnitude due to the hexapole-selection. This is the most disadvantageous point when we wish to use oriented molecular beam. This project aims at resolving this weak point by developing a sophisticated method so-called "Electrostatic Honeycomb Field" for intensifying oriented molecular beam. Basic idea of the method is that a beam intensity is simply proportional to the number of beam lines and they can be focused on a point in space after the hexapole state-selection.

Figure 1 (top) shows photo views of the newly developed honeycomb electric field. The electric field consists of 24 pieces of electrodes which form seven sets of hexapole electric field lines. The seven beam lines are pointing at a point in downstream. Figure 1 (bottom) shows the schematic illustration of the apparatus. Seven sets of pulse valves (1 mmϕ), beam skimmer (1 mmϕ), and beam collimator (5 mmϕ) followed by the honeycomb field (1 m long), are mounted on four pieces of supporting stainless rods (15 mmϕ). All beam lines focus on to a point in the 1 m forward distance from the honeycomb filed. The honeycomb electrode is made from carbon fiber (CFPR pipe, 15 mmϕ, 7.5 mmϕ, 1 m long). Carbon fiber is chosen because of its light weight and high electric conduction. Polyacetal insulator is used as the electrode supporter. Beam intensity is monitored by a quadrupole mass spectrometer. As a preliminary experiment, we made comparison of the beam intensity between single-beam run and seven-beam run, and we obtained the expected beam enhancement. Additionally, we have obtained the focusing effect for acetonitrile molecule (CH_3CN, $\mu = 3.92$ D) by use of honeycomb electric field for the first time. We are now doing to optimize the operating in order to get the most intensisve oriented molecular beam.

Reference

1) "*Steric Effects in Small Radical Formations*," in The *Chemical Dynamics and Kinetics of Small Radicals, Part II*, K. Liu and A. Wagner, Eds., Advanced Series in Physical Chemistry (World Scientific), K. Kuwata, and T. Kasai, Vol. **6**, 842-935 (1995)

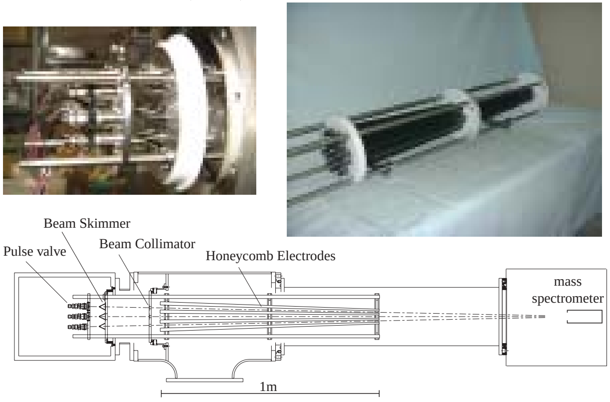

Figure 1. Honeycomb type orientational state selector. The beam source and the honeycomb electric field (top) and a schematic view of the newly designed apparatus for intense oriented molecular beam (bottom).

Ultraviolet Synchrotron Orbital Radiation Facility

VIII-J Development of the UVSOR Light Source

VIII-J-1 UVSOR Upgrade Project

KATOH, Masahiro; HAYASHI, Kenji; HONDA, Toru[1]; HORI, Yoichiro[2]; HOSAKA, Masahito; KINOSHITA, Toshio; KODA, Shigeru; TAKASHIMA, Yoshifumi; YAMAZAKI, Jun-ichiro; KITAMURA, Hideo[3]; HARA, Toru[3]; TANAKA, Takashi[3]
([1]KEK-PF; [2]IMS and KEK-PF; [3]RIKEN)

Towards upgrading UVSOR, we have designed a new magnetic lattice, in which the beam emittance would be reduced and the number of the straight sections available for insertion devices would be doubled. The accelerator components necessary for the upgrade project are under development. A combined function magnet was designed, which is capable of producing both quadrupole field and sextupoles filed. A prototype was constructed and the field measurements are in progress. Some early results have shown that the required field strengths could be achieved. The beam position monitor system was replaced and successfully commissioned. The new system can measure one orbit in a second with resolution of a few microns. It will be a powerful tool in stabilizing the low emittance electron beam. An in-vacuum undulator is under construction. This will be installed in the ring, in spring, 2002, to check the performance and the effects on the electron beam. This type of device is expected to provide SR beams of higher brilliance in higher energy region above 100 eV.

VIII-J-2 Storage Ring Free Electron Laser

KATOH, Masahiro; GEJO, Tatsuo; HAMA, Hiroyuki[1]; HAYASHI, Kenji; HOSAKA, Masahito; KINOSHITA, Toshio; KODA, Shigeru[2]; SHIGEMASA, Eiji; TAKASHIMA, Yoshifumi; YAMAZAKI, Jun-ichiro
([1]Tohoku Univ.; [2]IMS and Saga Univ.)

The storage ring free electron laser (FEL) at UVSOR has successfully oscillated in the wide spectral region from 590 nm to 240 nm. In these years, we have made many efforts to realize stable oscillation and high average power. As the result, the average power has exceeded 1 W, which is the world highest record as a storage ring FEL. One of the unique features of the storage ring FEL is the natural and perfect pulse-to-pulse synchronization with the synchrotron radiation pulses, which are produced in the same storage ring. By utilizing this, we have performed a pump-probe experiment, in which SR pulses from an undulator excite Xe atoms and the excited state with 1 nsec lifetime was probed by the FEL pulses.

VIII-J-3 Vacuum System Remodeling for the UVSOR Upgrading

HORI, Yoichiro; YAMAZAKI, Jun-ichiro; KATOH, Masahiro; HAYASHI, Kenji; HOSAKA, Masahito; KINOSHITA, Toshio

The beam lifetime of the UVSOR depends strongly upon both bunch size and pressure. Because a high brilliance is obtained by reducing the bunch size in the UVSOR upgrading plan designed at present, the lower operating pressure should be achieved to maintain a long beam lifetime. This project purposes to improve the present vacuum condition and to achieve the required operating pressure in the upgraded ring. We have started observation and inspection of the vacuum situation of the ring. Also the design of new beam chambers for the upgraded ring has been undertaken, where reinforcing the pumping speeds and increasing the beam position monitor are considered.

VIII-K Researches by the USE of UVSOR

VIII-K-1 Photo-Induced Phase Transition of Spin-Crossover Complex Studied by Photoelectron Spectroscopy

KAMADA, Masao; DOI, Yo-ichiro[1]; TAKAHASHI, Kazutoshi; FUKUI, Kazutoshi[1]; TAYAGAKI, Takeshi[2]; TANAKA, Koichiro[2]
([1]Fukui Univ.; [2]KyotoUniv.)

The photo-induced phase transition (PIPT) of an organometal spin-crossover complex $[Fe(2\text{-pic})_3]Cl_2\cdot$EtOH has been studied by photoelectron spectroscopy. The Fe-3d and N-1s spectra showed remarkable changes due to the photo-excitation at low temperatures, indicating that the electron charge is transferred from nitrogen to Fe atoms in the PIPT. The electronic structure of the photo-induced phase is very different from that of the high-temperature phase, which is caused by thermally induced phase transition (TIPT). The valence-band spectra of the photo-induced phase is in good agreement with the cluster calculation involving the E_g-distortion of Fe-octahedrons, indicating that the symmetry lowering in the excited state plays an important role to cause the PIPT. It was also found that the valence-band spectra are enhanced around T_c's, indicating the dynamics of the PIPT competing with the

TIPT.

VIII-K-2 Beam-Line Systems for Pump-Probe Photoelectron Spectroscopy Using SR and Laser

KAMADA, Masao; TANAKA, Senku; TAKAHASHI, Kazutoshi; DOI, Yo-ichiro[2]; FUKUI, Kazutoshi[2]; KINOSHITA, Toyohiko[3]; HARUYAMA, Yuichi[4]; ASAKA, Shuji; FUJII, Yasuo[1]; ITOH, Minoru[5]
([1]Osaka City Univ.; [2]Fukui Univ.; [3]ISSP, Univ. Tokyo; [4]Himeji Inst. Tech.; [5]Shinshu Univ.)

[*SRI proceedings* (2001)]

Since the first report by Saile, several groups have been developing new spectroscopy based on the combination of synchrotron radiation and laser light. The new spectroscopy are very attractive and interesting, since both synchrotron radiation and laser light are useful light sources with different characteristics: Synchrotron radiation provides high photon energy to investigate core-levels, while laser light is so intense to produce excited valence states with high density. Various combinations of two powerful light sources may open new scientific achievements. Combined systems for photoelectron spectroscopy using synchrotron radiation and laser light have been constructed at BL 5A and BL6A2 in the UVSOR facility, Okazaki. The systems consist of high-performance photoelectron spectrometers and mode-locked lasers. The performance of the systems is reported with a few examples.

VIII-K-3 Experiments with Combined Laser and SR at the UVSOR Facility

KAMADA, Masao

[*LSWAVE proceedings* (2001)]

There are several ways to use SR and Laser. One is to use SR as pump and laser as probe. This is powerful to investigate many interesting phenomena concerning with core-level excitations. Second is to use laser as pump as SR as probe. This is very useful to investigate many phenomena relating with valence excitations. Third one is to use SR and laser simultaneously as 2-photon excitation. This will open the new science relating with core-level excitation too. In recent years, brilliance of SR is increased and also short- wavelength lasers are under progress. So, many persons may expect more combinations in near future such as SR-Pump + SR-Probe, Laser-Pump + Laser-Probe, Laser 2-Photon-Pump, and SR 2-Photon-Pump.

VIII-K-4 Cesiumoxide-GaAs Interface and Layer Thickness in NEA Surface Formation

MORÉ, Sam Dylan; TANAKA, Senku[1]; NISHITANI, Tomohiro[2]; NAKANISHI, Tsutomu[2]; KAMADA, Masao
([1]GUAS; [2]Nagoya Univ.)

[*PES proceedings* (2001)]

Negative electron affinity (NEA) surfaces have found applications as efficient photocathodes and the NEA surface of GaAs(100) and its superlattice is known to be a useful emitter of spin-polarized electrons with a high degree of polarization and efficiency. This can be achieved by the ‘jo-jo’-technique, where Cs deposition and subsequent oxidation are repeated several times. The details of NEA surface formation, however, are not fully understood: previous reports differ considerably both in describing the method of production as well as the underlying chemical and physical mechanism. In this paper we present a systematic study of various sample treatments on GaAs(100) using photoemission spectroscopy. Analyzing the influence of the both the cesiation and oxidation on the bandbending and monitoring the photoemission yield on bulk GaAs(100), we have been able to distinguish three different regimes of activation, depending on the total thickness of the overlayer, the Cs:O ratio and the resulting chemical interaction with the substrate.

VIII-K-5 Surface Photovoltage Effects on *p*-GaAs (100) from Core-Level Photoelectron Spectroscopy Using Synchrotron Radiation and a Laser

TANAKA, Senku[1]; MORÉ, Sam Dylan; MURAKAMI, Junichi[2]; ITOH, Minoru[2]; FUJII, Yasuo[3]; KAMADA, Masao
([1]GUAS; [2]Shinshu Univ.; [3]Osaka City Univ.)

[*Phys. Rev. B* (2001) in press]

The surface photo-voltage (SPV) effect on laser-excited *p*-GaAs (100) has been investigated using core-level photoelectron spectroscopy with synchrotron radiation (SR). The energy shift of the Ga-*3d* photoelectrons due to the SPV effect was remarkably dependent on the sample temperature and the laser photon-flux. The dependence in each case was well interpreted on the basis of a simple SPV formula derived from the band-bending scheme with excess photocarriers. The magnitude of the band bending was about 0.8 eV for clean *p*-GaAs (100) surfaces having no electrodes. Similar core-level shifts were observed in the Ga-3*d* and Cs-4*d* spectra of Cs/GaAs (100), indicating an unpinned behavior of the electronic states of the Cs surface layer. The time response of the SPV effect was also investigated in the nano-second range using a pump-probe method with SR and laser.

VIII-K-6 Performance Tests for the Newly Constructed Varied-Line-Spacing Plane Grating Monochromator at BL-4B

SHIGEMASA, Eiji; NAGASONO, Mitsuru; OJI, Hiroshi; HATSUI, Takaki; GEJO, Tatsuo; KOSUGI, Nobuhiro

The practical construction of the new Varied-line-spacing Plane Grating Monochromator (VLS-PGM) on BL4B at the UVSOR has begun, in order to realize various spectroscopic studies with high resolution in the soft x-ray range (100~1000 eV). The installation has been successfully finished in October 2000. The vacuum condition was ready for obtaining the first SR light before the end of December 2000, and the first performance tests for the monochromator have been carried out.

The absolute photon flux for two gratings available so far (267 and 800 l/mm) has been measured using a Si photodiode supplied by IRD Inc. With the entrance and exit slit openings set at 25 and 10 µm, corresponding to the resolving power of 10000 at 400 eV with the 800 l/mm grating, the photocurrent from the photodiode was measured after the sample position, and converted into the absolute photon flux, taking account of the quantum efficiency of the photodiode. In this case, the resolving power in the regular spectral region for each grating is more than 3000. The throughput photon flux measured ranges from 10^8 to 10^9 photons/sec for the ring current of 100 mA, which is a little smaller than that estimated.

The inner-shell photoabsorption spectra of atoms and molecules were measured, to examine the instrumental resolution. The *K*-shell photoabsorption spectrum of N_2 is presented in Figure 1. The entrance and exit slits were set for achieving the resolving power of 10000. From the comparison with all available spectra of the N 1s → π* resonance of N_2, it seems to be reasonable that the resolving power obtained here is more than 5000. The photoabsorption spectra in the vicinity of the 2p ionization thresholds of S (~170 eV) for H_2S, OCS, SO_2, and CS_2 were also recorded using the 267 l/mm grating. Through the performance tests, it turned out that the resolving power more than 3000 is achieved at the entire photon energy region of interest.

Figure 1. K-shell photoabsorption spectrum of N_2.

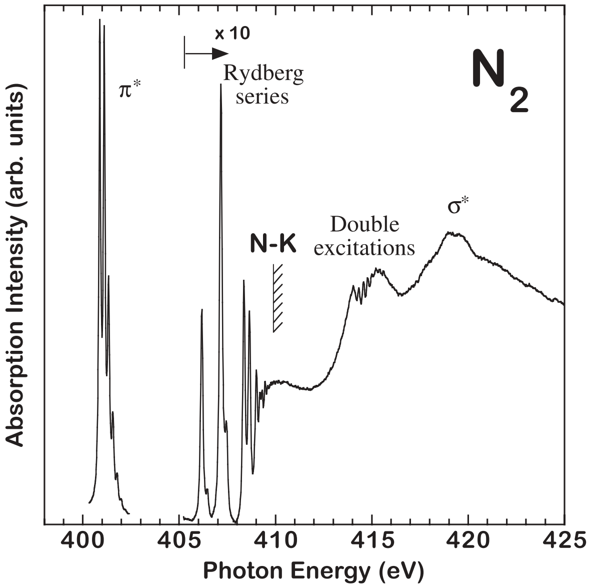

VIII-K-7 High-Resolution Symmetry-Resolved K-Shell Photoabsorption Spectra of N_2

SHIGEMASA, Eiji; NAGASONO, Mitsuru; OJI, Hiroshi; HATSUI, Takaki; GEJO, Tatsuo; KOSUGI, Nobuhiro

High-resolution angle-resolved ion-yield spectra of N_2 have been measured using linearly polarized synchrotron radiation. The ion yield spectra (I_0 and I_{90}) measured at 0 and 90 degrees with respect to the electric vector of the light relate to the Σ ($\Delta\Lambda = 0$) and Π ($\Delta\Lambda = \pm 1$) symmetry components in the conventional photoabsorption spectrum, respectively. The Σ and Π symmetry spectra in the vicinity of the *K*-shell ionization threshold of N_2, except for the π* resonance are shown in Figure 1. Clear decomposition of the conventional photoabsorption spectrum into its symmetry components is observed. Concentrating on the *K*-shell ionization region, structures labeled from A to F, which are considered as being due to the multiple excitations, can be seen in the Σ and Π symmetry spectra. A strong and broad enhancement due to the σ* shape resonance, which is a typical single electron transition in the continuum, is found only in the Σ symmetry spectrum. A very weak structure B just above the ionization threshold, and a shoulder structure E of the shape resonance enhancement are observed in the Σ spectrum. In the Π symmetry spectrum, a structure A just above the ionization threshold, rather strong features C and D at the double excitation region, and a clear enhancement F just at the shape resonance position are detectable.

In order to elucidate the electronic structures of the spectral features observed in Figure 1, ab initio SCF-CI calculations have been performed, taking account for the transitions from $2\sigma_u$, $3\sigma_g$, and $1\pi_u$ orbitals into $1\pi_g$ (π*) orbital. As a consequence, it is found that the structure labeled F in the Π spectrum just at the shape resonance position is attributable to the triple excitations, where a simultaneous excitation of two valence electrons follows the inner-shell excitation.

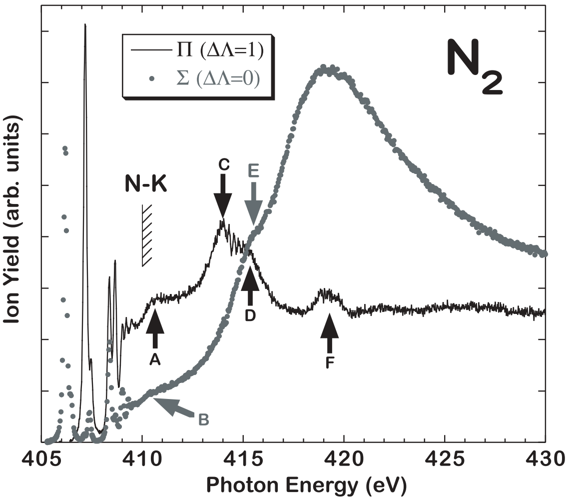

Figure 1. Symmetry-resolved K-shell photoabsorption spectrum of N_2.

VIII-K-8 Dynamical Angular Correlation in Molecular Auger Decay

GUILLEMIN, Renaud[1]; SHIGEMASA, Eiji; LE GUEN, Karine[1]; CEOLINE, Denis[1]; MIRON,

Cataline[1]; LECLERCQ, Nicola[1]; MORIN, Paul[1]; SIMON, Marc[1]
([1]LURE)

The first measurements of the angular distribution of Auger electrons from fixed-in-space molecules have been performed in the C *K*-shell ionization region of CO, for both parallel and perpendicular orientation of the molecular axis with respect to the light polarization vector. The ions emitted parallel or perpendicular to the electric vector of the incident radiation determine the possible Σ or Π symmetries in the ionization channels, respectively. The angular distributions obtained for the CO^{2+} $B^1\Sigma$ Auger final state show dramatic spectral variations, which also depend on the initial ionization channels, Σ or Π. The result strongly suggests the breakdown of the two-step model in which the Auger decay is treated independently of the initial photoionization process.

VIII-K-9 Pump /Probe Experiments with FEL and SR Pulses at UVSOR

GEJO, Tatsuo; SHIGEMASA, Eiji; NAKAMURA, Eiken; HOSAKA, Masahito; KODA, Shigeru; KATOH, Masahiro; YAMAZAKI, Jun-ichiro; HAYASHI, Kenji; TAKASHIMA, Keiji; HAMA, Hiroyuki[1]
([1]Tohoku Univ.)

Synchrotron radiation free electron lasers (SRFEL or FEL) has been used as a light source because of high power, high coherence and its unique temporal feature. Pump and probe experiments using FEL and synchrotron radiation (SR) pulses have been tried to perform for the last decade. This is due to the fact that the FEL pulse naturally synchronizes with the SR pulse. As the first gas-phase experiment combined FEL with SR, we have carried out the two-photon double-resonant excitation on Xe atoms, utilizing a SR pulse as a pump and an FEL pulse as a probe light.

The experiments were performed on the undulator beamline BL3A1 at UVSOR, where no monochromator is installed. An LiF filter was employed to suppress higher harmonics radiation from the undulator. The estimated photon flux is about 10^{13} photons/sec/0.1% B.W. at I = 100 mA. The FEL pulses were extracted through the backward mirror and transported to an experimental station of the BL3A1 through a series of multi-layer mirrors. The flight path of FEL, which was adjusted to synchronize timing between the FEL and the SR pulses, was about 30 m. A focusing mirror (f = 10 m) was placed in the center of the flight path to keep the beam size of FEL small throughout the transport. About 69% of the extracted power was transferred to the experimental station. The fine adjustment of the delay timing was made by using a movable optical delay system (50 cm) at the experimental station. The FEL and SR pulses introduced coaxially crossed an effusive jet of Xe atoms from a gas nozzle. The singly charged Xe ions produced in the interaction region were detected by means of a conventional channeltron.

The first experiment on the two-photon double-resonant excitation of the Xe* $5p^5nf$ autoionization states using the combination of a mode-locked laser and SR has already been successfully demonstrated by Meyer's group at LURE.[1)] In the present work, the combination of FEL and the undulator radiation was chosen in place of the former. The fundamental harmonic of the undulator was adjusted to be 10.4 eV, in order to prepare the Xe* $5p^55d$ intermediate states in a first step. The Xe* $5p^54f$ autoionization resonance can be excited within the wavelength region of FEL in a second step. Because the lifetime of the intermediate states is quite short (600 ps), the synchronization between the SR and laser pulses is essential in this experiment.

The ion yield spectrum for the autoionization Xe* $5p^54f$ resonance obtained as shown in Figure 1. In this measurement the wavelength of FEL was swept by changing the gap of the helical optical klystron. During the measurement a newly developed feedback system was operated to stabilize the lasing. The asymmetric line shape described by the Fano formula has been clearly observed in Figure 1.

We are going to perform the same experiment at the beamline BL7B, where a high-resolution monochromator is installed, to improve the spectral resolution.

Reference

1) M. Gisselbrecht, A. Marquette and M. Meyer, *J. Phys. B: At., Mol. Opt. Phys.* **31** L977 (1998).

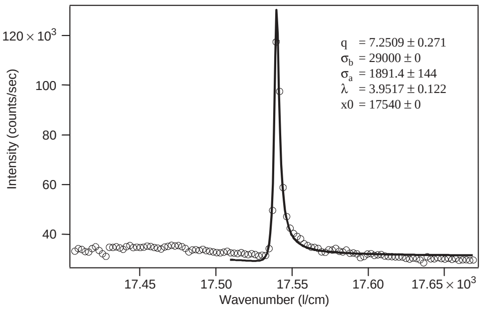

Figure 1. Two-photon ionization signal of Xe as a function of the wavelength of FEL.

Computer Center

VIII-L Theoretical Studies on Electronic Structure and Dynamics of Electronically Excited States in Polyatomic Molecules

VIII-L-1 Quantum Reactive Scattering Calculations of the O(^{1}D) + HCl Reaction Using the Global ab initio Potential Energy Surfaces of Electronic Excited States

NANBU, Shinkoh; BIAN, Wensheng; KAMISAKA, Hideyuki[1]; AOYAGI, Mutsumi; TANAKA, Kiyoshi[2]; NAKAMURA, Hiroki
([1]GUAS; [2]Hokkaido Univ.)

The O (^{1}D) + HCl ($^1\Sigma^+$) reaction is quite important due to the significant role in stratospheric chemistry. The reaction is correlated with five electronic states, and there are two product channels, OH ($^2\Pi$) + Cl (^{2}P) and ClO ($^2\Pi$) + H (^{2}S) if its spin-symmetry is kept. Up to now, ab initio calculations of the ground PES and quantum wave packet calculations have been carried out along that surface, although at least three electronic potential energy surfaces are involved in this reaction.

In the present work, we have determined new global three ab initio potential energy surfaces accurately; and furthermore quantum wave packet dynamics calculations have been carried out to obtain the total reaction probabilities. The reaction probability for HCl (v = 0, j = 0) shows that the OH + Cl product channel via the 1^1A” state should be opened at the lower collision energy than $E_{\rm coll}$ = 0.529 eV, while the channel via 2^1A’ should be closed. Although there was the discrepancy between previous theoretical works and experimental results, it was explained by our works including the electronic excited states.

VIII-L-2 Millimeter-Wave Spectroscopy of the Internal-Rotation Band of the He–HCN Cluster and Determination of the Empirical Intermolecular Potential Energy Surface

HARADA, Kensuke[1]; TANAKA, Keiichi[1]; TANAKA, Takehiko[1]; NANBU, Shinkoh; AOYAGI, Mutsumi
([1]Kyusyu Univ.)

[*J. Chem. Phys.* submitted]

Millimeter-wave absorption spectroscopy was applied to the measurement of the internal-rotation band of the He–HCN cluster in the frequency region of 95–125 GHz. In total 13 rovibrational lines, split into nitrogen nuclear hyperfine structure, were observed for the fundamental internal-rotation band, j = 1–0.

In order to determine the empirical intermolecular potential energy surface (PES), the potential parameters were optimized by the Newton-Raphson method; the exact Schrödinger equation for the weekly bound complex was solved, and then the derivatives were evaluated. The obtained PES has a global minimum in the linear configuration (He$\cdots$H–C–N) with a well depth of 27.827 cm^{-1}, and the saddle point located in the anti-linear configuration (H–C–N$\cdots$He) is higher in energy than the global minimum by 8.174 cm^{-1}. The distance $R_{\rm m}$ from the He atom to the center of mass of HCN along the minimum energy path shows a large angular dependence; $R_{\rm m}$ = 4.211 Å and 4.104 Å in the linear and anti-linear forms, respectively, and has a minimum value of 3.513 Å in a T-shaped configuration. The rovibrational energies calculated from the empirical PES suggest that the cluster will dissociate at l = 5 in the first excited internal-rotation state, j = 1, where l denotes the quantum number for the end-over-end rotation of the cluster. This is consistent with the millimeter-wave observation of sudden disappearance of the first excited state of the intermolecular stretching vibration is located just below the dissociation limit, –0.202 cm^{-1}.

VIII-L-3 Determination of the Global Potential Energy Surfaces and Transition Wave Packet Dynamics for Polyatomic Systems

NANBU, Shinkoh; ISHIDA, Toshimasa[1]; GRAY, Stephen K.[2]; AOYAGI, Mutsumi
([1]Shizuoka Univ.; [2]Argonne Natl. Lab.)

Computational algorithm for the determination of the global potential energy surfaces of polyatomic systems are developed with using the interpolant moving least squares scheme, which was proposed by Ishida and Schatz [*Chem. Phys. Lett.* **314**, 369 (1999)]. In this sheme, any derivatives in quantum-chemical calculations are not required to construct the surface and in contrast with previously developed shemes based on Shepard interpolation alone. In our new algorithm, the molecular conformations are generated with the Monte Carlo sampling, and then the ab initio calculations for all of the conformations are performed by parallel computing. Therefore, we have good advantage for computational time for the serial calculations. Application is made to the tetra-atomic systems, the 2OH ↔ H_2O + O reaction.

Regarding to the wave packet dynamics, we are also developing the program code based on the MPI-library to make a time-evolution of the wave packet for the tetra-atomic systems.

VIII-L-4 Ab Initio Study of p-tert-Butylcalix[4]crown-6-ether Complexed with Alkyl Ammonium Cations

CHOE, Jong-In[1]; CHANG, Suk-Kyu[1]; WOOK

HAM, Seung[1]; NANBU, Shinkoh; AOYAGI, Mutsumi
([1]Chung-Ang Univ.)

[*Bull. Korean Chem. Soc.* **22**, 356 (2001)]

The conformations and energies of *p-tert*-butylcalix-[4]crown-6-ether (**1**) and its alkyl ammonium complexes have been calculated by *ab initio* (6-31G) quantum mechanics method. The cone conformation was found to be most stable for free host **1**. We have determined the binding site of these host-guest complexes focusing on the crown-6-ether or *p-tert*-butylcalix[4]arene pocket of the cone conformation of host molecule **1**. The primary binding site of host **1** for the recognition of alkyl ammonium guests was confirmed to be the central part of the crown moiety of cone conformation. The complexation energy calculations revealed that the ammonium cation without alkyl group showed the better complexation efficiency when combined with host **1**, that is in satisfactory agreement with the experimental results.

VIII-L-5 Nonadiabatic Process in Nonintegrable Quantum Systems

TAKAMI, Toshiya

We study nonadiabatic processes in classically nonintegrable systems. We have shown that extra-transitions arise from nonadiabatic couplings between eigenstates on the endpoints, and that, paradoxically, the usual adiabatic base is useless in the adiabatic limit to observe Landau-Zener transition. In order to describe the extra-transition theoretically, we introduce “boundary expansion” to obtain higher order terms of the nonadiabatic couplings. By the use of the expansion, we construct a new base which can describe non-adiabatic transition locally even in nonintegrable systems. This base is shown to be an extension of the superadiabatic base which is known as an asymptotic approximation of the exact solution. While our approach above is only for simple time-dependent nonadiabatic systems, we consider in the next applying the super-adiabatic analysis to chemical reactions. In order to analyze nonadiabatic processes on molecules in the adiabatic limit, we introduce the phase-space analysis through the method of the adiabatically renormalized Hamiltonian.

VIII-L-6 Theoretical Study of Endohedral Metalofullerene La@C_{76}

MAKI, Jun; AOYAGI, Mutsumi; KATO, Tatsuhisa; OKUBO, Shingo[1]
([1]GUAS)

Endohedral metallofullerenes have attracted interests as new molecules having novel properties. We have carried out DFT calculation to get information on cage structure of La@C_{76}. Two IPR satisfying structures with T_d and D_2 symmetries are possible for C_{76} cage, while it has known from the ^{13}C NMR that empty C_{76} has D_2 symmetry. The result of geometry optimizations showed that La@C_{76} with T_d-cage is more stable. Theoretical IR spectrum of D_2-C_{76} reasonably reproduced experimental one of sublimed C_{76} films, although it was difficult to compare it with our measured IR spectra in CS_2.

VIII-L-7 Formation of HCl^+ ($A^2\Sigma^+$) and HBr^+ ($A^2\Sigma^+$) Resulting from He (2^3S) Penning Ionization of HCl and HBr

TOKUE, Ikuo[1]; TANAKA, Hiroyuki[1]; YAMASAKI, Katsuyoshi[1]; NANBU, Shinkoh
([1]Niigata Univ.)

[*J. Phys. Chem. A* submitted]

He (2^3S) Penning ionization of HCl and HBr leading to HCl^+ (A) and HBr^+ (A) has been studied optically by using a crossed-beam apparatus. The ratios of the vibrational population, $P_{v'}/P_v$ (v' = 2 and 3) of HCl^+ (A) and P_1/P_0 of HBr^+ (A), increase with the collision energy in the region of 120–200 meV. The rotational distributions of HCl^+ (A, v' = 0) and HBr^+ (A, v' = 0) can be represented by a double-Boltzmann distribution; the temperatures are 200 ± 50 and 700 ± 80 K for HCl^+ (A, v' = 0) and 250 ± 50 and 1200 ± 200 K HBr^+ (A), and are nearly independent of the collision energy. The model potential surface for He*(Li) + HCl as the entrance channel is nearly isotropic and shows a shallow dip of about 20 meV, while the surface for He + HCl^+ (A) as the exit channel is anisotropic and shows a deep minimum of 250 meV in the He–H–Cl collinear direction. These results suggest that at least two processes contribute to formation of these ions; one is the direct Penning ionization and the other is the formation via a temporary complex $[HeHCl(A)]^+$ by orbiting.